

# Subgap features due to quasiparticle tunneling in quantum dots coupled to superconducting leads

Sebastian Pfaller,<sup>\*</sup> Andrea Donarini, and Milena Grifoni  
*Theoretische Physik, Universität Regensburg, 93040 Regensburg, Germany*  
 (Dated: August 31, 2012)

We present a microscopic theory of transport through quantum dot set-ups coupled to superconducting leads. We derive a master equation for the reduced density matrix to lowest order in the tunneling Hamiltonian and focus on quasiparticle tunneling. For high enough temperatures transport occurs in the subgap region due to thermally excited quasiparticles, which can be used to observe excited states of the system for low bias voltages. On the example of a double quantum dot we show how subgap transport spectroscopy can be done. Moreover, we use the single level quantum dot coupled to a normal and a superconducting lead to give a possible explanation for the subgap features observed in the experiments of Ref. 1.

PACS numbers: 73.23.Hk, 73.63.Kv, 74.45.+c

## I. INTRODUCTION

In the last two decades modern fabrication techniques made it possible to connect quantum dot systems with superconducting leads. Quantum dots were realized with carbon nanotubes<sup>1–7</sup>, metallic particles<sup>8</sup>, semiconducting nanowires<sup>9–12</sup>, single fullerene molecules<sup>13</sup>, self-assembled nanocrystals<sup>14</sup> and graphene quantum dots<sup>15</sup>. The experiments show a gap in the Coulomb diamonds which is proportional to the superconducting gap, reflecting the BCS-density of states. In the sequential tunneling regime higher order quasiparticle tunneling processes are suppressed and current flows due to single quasiparticle tunneling. First transport theories were presented<sup>16</sup>, using a master equation approach, where the rates were calculated on the basis of Fermi's golden-rule. Another method based on non-equilibrium Green's function was used by Yeyati *et al.*<sup>17</sup> and K. Kang<sup>18</sup> to describe resonant tunneling through an effective single level quantum dot in the limit of very strong Coulomb repulsion in the dot ( $U \rightarrow \infty$  limit), where transport is governed by quasiparticle tunneling; the corresponding I-V curves show an intrinsic broadening of the BCS-like feature in the current in agreement with experimental observation<sup>8</sup>. For small Coulomb repulsion, higher order processes lead to Josephson current<sup>9</sup> and Andreev reflections<sup>2–5,7,10,15</sup>, which appear as subgap features in the experiments. Both effects were studied intensely experimentally and theoretically<sup>4,17,19,20</sup> and were recently summarized in review articles of Refs. 21 and 22. Besides Andreev reflections also the Kondo effect<sup>13</sup> as well as Yu-Shiba-Rusinov bound states<sup>5,23,24</sup> can lead to subgap features and are subject of current research. If the temperature becomes comparable with the superconducting gap quasiparticles can get thermally excited across the gap, leading to additional subgap features<sup>16</sup>.

In the following we present a microscopic theory for transport through superconducting hybrid nanojunctions for finite superconducting gap  $|\Delta| < \infty$  in the sequential tunneling limit. In particular, we trace out all degrees of freedom of the superconducting leads to obtain a gen-

eralized master equation for the reduced density matrix to lowest order in the tunneling Hamiltonian. In contrast to Green's function techniques, see e.g. Ref. 22, this method enables to treat the interactions on the system *exactly*. Moreover, as shown on the example of a double quantum dot, our theory can treat any quantum dot set-up if its many-body energy spectrum and eigenstates are known. We focus on transport involving thermally excited quasiparticles, and show that excited states of the quantum dot system can be observed in the current voltage spectroscopy in the Coulomb blockade region. Though transitions between two ground states are blocked due to the gap in the BCS-density of states, thermally excited quasiparticles can participate in transport through excited system states, giving a source of subgap features in superconducting hybrid systems. For a quantum dot coupled to a normal and a superconducting lead, a possible explanation for the subgap features observed in Ref. 1 is given, where a carbon nanotube quantum dot is coupled to a normal and a superconducting contact.

The manuscript is organized as follows: In Sect. II we introduce the Hamiltonian in a system-bath model using a number conserving version of the Bogoliubov-Valatin transformation<sup>25,26</sup> to describe the electrons of the superconducting leads as quasiparticle excitations of the BCS-ground state and Cooper pairs, introducing Cooper pair creation and annihilation operators. The Cooper pair operators are essential to conserve the total particle number and have important consequences on the transport properties. In Sect. III we derive an explicit form of the Cooper pair operators following Ref.<sup>27</sup> and discuss the influence on thermodynamic properties of the leads. In Sect. IV, the general master equation for the reduced density matrix is derived and used to calculate the current. In Sect. V we use the theory to calculate transport characteristics for two systems, the single level quantum dot (SD) and the double quantum dot (DD), the later in two possible configurations cf. Fig. 1. The SD is used to explain basic phenomena like a gap opening in the Coulomb diamonds which is proportional to the superconducting gap, and transport involving ther-

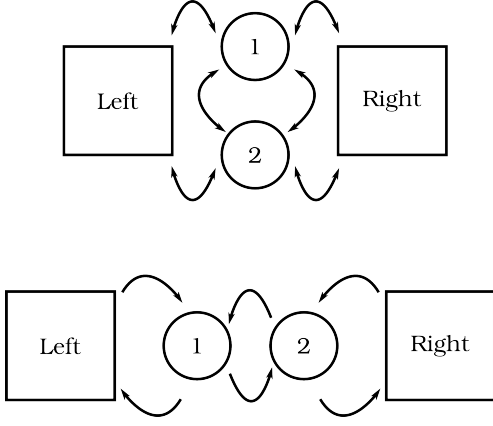


Figure 1. Sketch of the transport set-up of a double quantum dot (DD) coupled to superconducting leads. The DD is illustrated in the parallel (top panel) and serial (bottom panel) configuration. Tunneling events are depicted by arrows.

mally excited quasiparticles<sup>16</sup>. On the other hand, the DD possess a richer many-body spectrum with several excited states. We visualize transitions through excited system states in the low bias regime using thermally excited quasiparticles. Due to the gap in the BCS-density of states, the ground state to ground state transition is not allowed in all cases, leading to transport through excited system states, appearing as peaks *in* the Coulomb blockade region. The threshold for observing excited system states in the subgap region is that the energy difference between the excited state and its ground state must be smaller than  $2|\Delta|$ . We confirmed this threshold by means of the independently gated DD, where the detuning of the two sites changes the level spacing. Finally the N-QD-S system is investigated, where a quantum dot is coupled to a normal and a superconducting lead. In this case only the superconducting lead produces thermal lines in the Coulomb blockade region, giving a possible explanation for the subgap features in Ref. 1.

## II. MODEL HAMILTONIAN

In the following we consider quantum dot systems weakly coupled to two superconducting leads. The total Hamiltonian is written in a system-bath model:

$$\hat{H} = \hat{H}_S + \hat{H}_B + \hat{H}_T, \quad (1)$$

where  $\hat{H}_S$  represents the Hamiltonian of the quantum dot system,  $\hat{H}_B$  is the Hamiltonian of the superconducting leads, and  $\hat{H}_T$  describes the tunneling between the system and the leads. Specifically, we focus on two systems, a single level quantum dot (SD) and a double quantum dot (DD). The SD has been focus of many theoretical works before<sup>16–20</sup>, and we use its simple Fock-space structure to demonstrate some generic effects resulting from the superconducting leads.

We describe the SD by the single impurity Anderson model:

$$\hat{H}_{SD} = \sum_{\sigma} \epsilon_d \hat{d}_{\sigma}^{\dagger} \hat{d}_{\sigma} + U \hat{n}_{\uparrow} \hat{n}_{\downarrow}, \quad (2)$$

where  $\hat{n}_{\sigma} = \hat{d}_{\sigma}^{\dagger} \hat{d}_{\sigma}$  is the number operator of the electrons on the dot with spin  $\sigma$ . This model describes a quantum dot with on-site energy  $\epsilon_d$  and Coulomb repulsion  $U$  which can be occupied by at most two electrons. The highest occupied state is defined as  $|2\rangle = \hat{d}_{\uparrow}^{\dagger} \hat{d}_{\downarrow}^{\dagger} |0\rangle$ , the one particle states are defined as  $|1\sigma\rangle = \hat{d}_{\sigma}^{\dagger} |0\rangle$ , and  $|0\rangle$  is the state with zero particles.

For the DD we use a modified version of the Pariser-Parr-Pople Hamiltonian<sup>28,29</sup>:

$$\begin{aligned} \hat{H}_{DD} = & \sum_{\substack{\alpha \in \{1,2\} \\ \sigma \in \{\uparrow, \downarrow\}}} \epsilon_{\alpha\sigma} \hat{d}_{\alpha\sigma}^{\dagger} \hat{d}_{\alpha\sigma} + \sum_{\sigma} \left( b \hat{d}_{1\sigma}^{\dagger} \hat{d}_{2\sigma} + b^* \hat{d}_{2\sigma}^{\dagger} \hat{d}_{1\sigma} \right) \\ & + \sum_{\alpha} U_{\alpha} \left( \hat{n}_{\alpha\uparrow} - \frac{1}{2} \right) \left( \hat{n}_{\alpha\downarrow} - \frac{1}{2} \right) + V (\hat{n}_1 - 1)(\hat{n}_2 - 1). \end{aligned} \quad (3)$$

Here,  $\hat{d}_{\alpha\sigma}^{\dagger}$  are the creation operators for an electron on site  $\alpha \in \{1, 2\}$  with spin  $\sigma$ . They define the number operators  $\hat{n}_{\alpha\sigma} = \hat{d}_{\alpha\sigma}^{\dagger} \hat{d}_{\alpha\sigma}$ . The operator  $\hat{n}_{\alpha} = \hat{n}_{\alpha\uparrow} + \hat{n}_{\alpha\downarrow}$  counts the number of electrons on site  $\alpha$ . In the general case we distinguish between the four on-site energies  $\epsilon_{\alpha\sigma}$  and between the on-site Coulomb interactions  $U_{\alpha}$ . Electrons on different sites interact through the inter-dot Coulomb interaction  $V$ ;  $b$  describes the hopping between the two sites. In our set-up the on-site energies can be controlled by capacitively coupled gate electrodes. In the case of site-independent on-site energies and on-site Coulomb interaction the Hamiltonian can be diagonalized analytically<sup>30,31</sup>.

The superconducting leads are described by the mean field form,  $\hat{H}_B^{MF}$  of the pairing Hamiltonian, where we additionally inserted a unity represented by a product of Cooper pair annihilation and creation operators,  $\hat{S}_{\eta} \hat{S}_{\eta}^{\dagger} = 1$ , which will be specified later in Sec. III. We find

$$\begin{aligned} \hat{H}_B^{MF} = & \sum_{\eta k \sigma} \xi_{\eta k} \hat{c}_{\eta k \sigma}^{\dagger} \hat{c}_{\eta k \sigma} + \sum_{\eta} \mu_{\eta} \hat{N}_{\eta} \\ & + \sum_{\eta k} (\Delta_{\eta} \hat{c}_{\eta k \uparrow}^{\dagger} \hat{c}_{\eta - k \downarrow}^{\dagger} \hat{S}_{\eta} + \Delta_{\eta}^* \hat{S}_{\eta} \hat{c}_{\eta - k \downarrow} \hat{c}_{\eta k \uparrow}) \\ = & \hat{H}_G + \sum_{\eta} \mu_{\eta} \hat{N}_{\eta}, \end{aligned} \quad (4)$$

where  $\xi_{\eta k} = \epsilon_k - \mu_{\eta}$  measures single particle energies  $\epsilon_k$  with respect to the electrochemical potential  $\mu_{\eta}$ , and  $\hat{N}_{\eta} = \sum_{k\sigma} \hat{c}_{\eta k \sigma}^{\dagger} \hat{c}_{\eta k \sigma}$  counts the number of electrons in lead  $\eta$ . Finally,  $\Delta_{\eta} = |\Delta_{\eta}| e^{i\phi_{\eta}} \equiv -\sum_l V_{lk} \langle \hat{S}_{\eta}^{\dagger} \hat{c}_{\eta - k \downarrow} \hat{c}_{\eta k \uparrow} \rangle$  denotes the superconducting gap

of lead  $\eta$ . Here  $\langle \bullet \rangle$  denotes a thermal average calculated self-consistently using the mean field Hamiltonian of Eq. 4.

The tunneling Hamiltonian,

$$\hat{H}_T = \sum_{\eta k \sigma \alpha} t_{\eta \alpha \sigma} \hat{c}_{\eta k \sigma}^\dagger \hat{d}_{\alpha \sigma} + t_{\eta \alpha \sigma}^* \hat{d}_{\alpha \sigma}^\dagger \hat{c}_{\eta k \sigma}, \quad (5)$$

describes the tunneling between the leads and the two sites of the DD, where the tunneling coefficients  $t_{\eta \alpha \sigma}$  depend on the lead, site, and spin index. Depending on the choice of the tunneling coefficients the DD is described in parallel or in serial configuration, see Fig. 1. For the single dot we skip the index  $\alpha$  in Eq. (5), as only one site is involved.

### A. Diagonalization of the lead Hamiltonian

The most famous way to diagonalize the mean field Hamiltonian,  $\hat{H}_G$ , of Eq. (4) was first introduced by Bogoliubov<sup>32</sup>. We are following Josephson and Bardeen<sup>25,26</sup> who modified the so called Bogoliubov transformation in a number conserving way. We adopt this idea and define the Bogoliubov transformation:

$$\hat{c}_{\eta k \sigma}^\dagger = u_{\eta k} \hat{\gamma}_{\eta k \sigma}^\dagger + \text{sgn } \sigma v_{\eta k}^* \hat{\gamma}_{\eta - k \bar{\sigma}} \hat{S}_\eta^\dagger, \quad (6)$$

where  $\bar{\sigma} = -\sigma$ . In Eq. (6)  $\hat{\gamma}_{\eta k \sigma}^\dagger$  creates a fermionic quasiparticle, often called bogoliubon, which is defined by

$$\{\hat{\gamma}_{\eta k \sigma}^\dagger, \hat{\gamma}_{\eta' k' \sigma'}\} = \delta_{\eta \eta'} \delta_{k k'} \delta_{\sigma \sigma'}, \quad (7)$$

$$\hat{\gamma}_{\eta k \sigma} |\text{GS}\rangle_\eta = 0. \quad (8)$$

Here  $|\text{GS}\rangle_\eta$  denotes the BCS ground state, or Cooper pair condensate of lead  $\eta$ . Bogoliubons are quasiparticle excitations of the Cooper pair condensate, meaning that the Cooper pair condensate is defined as the vacuum state of the bogoliubons, see Eq. (8). The Cooper pair creation operator  $\hat{S}_\eta^\dagger$  creates a Cooper pair in lead  $\eta$ . It has to be defined in such a way that the unitarity of the Bogoliubov transformation is conserved. The coefficients  $u_{\eta k}$  and  $v_{\eta k}$  are complex numbers and fulfill:

$$|u_{\eta k}|^2 + |v_{\eta k}|^2 = 1. \quad (9)$$

They read:

$$u_{\eta k} = \sqrt{\frac{1}{2} \left( 1 + \frac{\xi_{\eta k}}{|E_{\eta k}|} \right)}, \quad (10)$$

$$v_{\eta k} = e^{i\phi_\eta} \sqrt{\frac{1}{2} \left( 1 - \frac{\xi_{\eta k}}{|E_{\eta k}|} \right)}, \quad (11)$$

where  $\phi_\eta$  is the phase of the superconducting gap  $\Delta_\eta$ . Applying the transformation of Eq. (6) on Eq. (4) we obtain:

$$\hat{H}_B = \sum_{\eta k \sigma} E_{\eta k} \hat{\gamma}_{\eta k \sigma}^\dagger \hat{\gamma}_{\eta k \sigma} + E_G + \sum_{\eta} \mu_\eta \hat{N}_\eta. \quad (12)$$

In Eq. (12)  $E_{\eta k} = \sqrt{\xi_{\eta k}^2 + |\Delta_\eta|^2}$  denotes the quasiparticle energy, and  $E_G$  is a constant energy off-set, often referred to as the energy of the Cooper pair condensate. For later reference we note that the term  $\sum_{\eta} \mu_\eta \hat{N}_\eta$  is not included in the diagonalization procedure and is still written in terms of electron operators.

### III. THE BCS GROUND STATE AND ITS CONNECTION WITH THE COOPER PAIR OPERATORS

In the microscopic description of superconductive tunneling it is necessary to know the analytical form of the Cooper pair operators. In this section we show the connection between the Cooper pair operators and the BCS ground state by rewriting the BCS ground state as a coherent superposition of states with a fixed number of Cooper pairs. We start from<sup>33</sup>:

$$|\text{GS}\rangle = \prod_k (u_k + v_k \hat{R}_k^\dagger) |0\rangle, \quad (13)$$

where  $|0\rangle$  is the vacuum state and  $\hat{R}_k^\dagger = \hat{c}_{k\uparrow}^\dagger \hat{c}_{-k\downarrow}^\dagger$ . Exploiting the fermionic properties of the electron operators we can write:

$$\begin{aligned} |\text{GS}\rangle &= \prod_k u_k \exp \left( \sum_k \frac{v_k}{u_k} \hat{R}_k^\dagger \right) |0\rangle \\ &= \mathcal{N} \sum_{n=0}^{\infty} \frac{1}{n!} \left( \sum_k \frac{v_k}{u_k} \hat{R}_k^\dagger \right)^n |0\rangle. \end{aligned} \quad (14)$$

Eq. (14) can be written in a more compact form<sup>27</sup>,

$$|\text{GS}\rangle = \sum_{n=0}^{\infty} b_n |n\rangle, \quad (15)$$

by defining

$$b_n = \mathcal{N} \frac{a_n}{n!}, \quad (16)$$

$$|n\rangle = \frac{1}{a_n} \left( \sum_k \frac{v_k}{u_k} \hat{R}_k^\dagger \right)^n |0\rangle. \quad (17)$$

In App. A 1 we prove that  $|n\rangle$  contains  $2n$  electrons which form  $n$  Cooper pairs. In Eq. (17) we have introduced an additional coefficient

$$a_n = \left( \sum_k \frac{|v_k|^2}{|u_k|^2} \right)^{n/2}, \quad (18)$$

to normalize the states:

$$\langle n|m \rangle = \delta_{nm}. \quad (19)$$

Following Eq. (17) we define the Cooper pair creation operator:

$$\hat{S}^\dagger \equiv \frac{1}{a_1} \sum_k \frac{v_k}{u_k} \hat{R}_k^\dagger, \quad (20)$$

such that a state with  $n$  Cooper pairs is created by applying the Cooper pair creation operator  $n$  times on the vacuum:

$$|n\rangle = (\hat{S}^\dagger)^n |0\rangle. \quad (21)$$

As we see from Eqs. (15) and (21) the ground state of the bogoliubons is created by Cooper pair creation operators. Using Eq. (20) we can proof the following properties of the Cooper pair operators:

$$[\hat{S}^\dagger, \hat{S}] = 0, \quad (22)$$

$$\hat{S}^\dagger \hat{S} = 1, \quad (23)$$

$$[\hat{S}^\dagger, \hat{N}] = 2\hat{S}^\dagger, \quad (24)$$

and

$$[\hat{S}^\dagger, \hat{\gamma}_{k\sigma}] = 0. \quad (25)$$

From Eq. (25) it follows that the bogoliubon operators and the Cooper pair operators commute.

#### A. Thermodynamic properties of the leads

The description of electrons in terms of bogoliubons and Cooper pairs makes it necessary to discuss the thermodynamic properties of the superconducting leads. The chemical potential in this description is the same as for the electrons, since the unitary transformation conserves all electronic degrees of freedom. In the following we drop the lead index  $\eta$ , and consider only one lead.

In order to calculate thermal expectation values we use the equilibrium density matrix of a superconductor:

$$\hat{\rho}_B = \frac{e^{-\beta \hat{H}_G}}{Z_G}, \quad (26)$$

where  $\hat{H}_G = \hat{H}_B - \mu \hat{N}$ ,  $\beta$  is the inverse thermal energy, and  $Z_G$  is the partition function in the grand canonical ensemble. We find that the thermal expectation value of a pair of Bogoliubov quasiparticles is equal to the Fermi function:

$$\text{Tr}_B \left( \hat{\gamma}_{k\sigma}^\dagger \hat{\gamma}_{k\sigma} \hat{\rho}_B \right) = \frac{1}{e^{\beta E_k} + 1} = f^+(E_k), \quad (27)$$

where the trace is over many-body quasiparticle states

$$|\{n\}\rangle = |n_{k_1\sigma_1}, n_{k_2\sigma_2}, \dots\rangle = \mathcal{A} \prod_{(q\tau) \in \{n\}} \hat{\gamma}_{q\tau}^\dagger |\text{GS}\rangle. \quad (28)$$

The factor  $\mathcal{A}$  normalizes the many body state of Eq. (28), and  $\{n\}$  is a set of occupation numbers. We can see that tracing over the many body states includes the Cooper pair degrees of freedom through the ground state. Hence the trace includes *all* electronic degrees of freedom. The derivation can be found in App. B.

For later reference, it is important to know thermal expectation values of combinations of bogoliubon and Cooper pair operators, for instance:

$$\text{Tr}_B \left( \hat{S}^\dagger \hat{\gamma}_{k\sigma}^\dagger \hat{\gamma}_{k\sigma} \hat{\rho}_B \right) = f^+(E_k). \quad (29)$$

In fact, since the Cooper pair operator is commuting with the bogoliubon operators, see Eq. (25), we need to calculate the BCS-ground state expectation value of a single Cooper pair operator, which is equal to one in the thermodynamic limit, see App. B:

$$\langle \text{GS} | \hat{S}^\dagger | \text{GS} \rangle = 1. \quad (30)$$

#### IV. TRANSPORT THEORY AND THE GENERALIZED MASTER EQUATION

The expectation value  $\mathcal{O} = \langle \hat{\mathcal{O}} \rangle = \text{Tr}(\hat{\mathcal{O}} \hat{\rho})$  of any observable associated to an operator  $\hat{\mathcal{O}}$  can be evaluated once the total density operator  $\hat{\rho}$  is known, cf. Eq. (46) below. To this extent we start from the Liouville equation for the density operator in the interaction picture, see e.g.<sup>34</sup>:

$$i\hbar \frac{\partial}{\partial t} \hat{\rho}_I(t) = [\hat{H}_{T,I}(t), \hat{\rho}_I(t)]. \quad (31)$$

Eq. (31) can be formally integrated and reinserted back into itself,

$$\begin{aligned} i\hbar \hat{\rho}_I(t) &= [\hat{H}_{T,I}(t), \hat{\rho}_I(0)] \\ &- \frac{i}{\hbar} \int_0^t dt' [\hat{H}_{T,I}(t), [\hat{H}_{T,I}(t'), \hat{\rho}_I(t')]], \end{aligned} \quad (32)$$

which is still exact at this level and allows a perturbative treatment in the tunneling Hamiltonian  $\hat{H}_T$ .

Prior to time  $t = 0$  the bath and the system do not interact, meaning that the total density matrix of system and leads are decoupled:

$$\hat{\rho}_I(0) = \hat{\rho}_S(0) \hat{\rho}_B(0). \quad (33)$$

The density matrix of the leads,  $\hat{\rho}_B$ , can be described by the equilibrium thermodynamic expression shown in Eq. (26). Further we assume that the leads have so many degrees of freedom that they stay in thermal equilibrium

up to a correction of order  $\hat{H}_T$ . It is convenient to trace out the degrees of freedom of the leads and define the reduced density matrix:

$$\hat{\rho}_{red,I}(t) \equiv \text{Tr}_B \hat{\rho}_I(t). \quad (34)$$

In the Schrödinger picture, the master equation for the reduced density matrix reads:

$$\begin{aligned} \dot{\hat{\rho}}_{red}(t) = & \frac{i}{\hbar} [\hat{\rho}_{red}(t), \hat{H}_S] - \left(\frac{i}{\hbar}\right)^2 \hat{U}_0(t) \int_0^t dt' \times \\ & \times \text{Tr}_B \left( \left[ \hat{H}_{T,I}(t), \left[ \hat{H}_{T,I}(t'), \hat{\rho}_{red,I}(t') \hat{\rho}_B \right] \right] \right) \hat{U}_0^\dagger(t), \end{aligned} \quad (35)$$

where we neglect terms of order  $\mathcal{O}(\hat{H}_T^3)$  and  $\hat{U}_0(t) = e^{-\frac{i}{\hbar} \hat{H}_S t}$  is the time evolution operator of the unperturbed system.

### A. Superconducting leads

The features of the superconducting leads are revealed when using the Bogoliubov transformation (6) to express the tunneling Hamiltonian. This yields additional terms compared to normal conducting theory.

#### 1. Time evolution of the quasiparticles

To proceed we have to specify the time evolution of the Bogoliubov and Cooper pair operators. We find:

$$\hat{\gamma}_{\eta k \sigma, I}^\dagger(t) = e^{+\frac{i}{\hbar}(E_k + \mu_\eta)t} \hat{\gamma}_{\eta k \sigma}^\dagger, \quad (36)$$

$$\hat{S}_{\eta, I}^\dagger(t) = e^{+\frac{i}{\hbar} 2\mu_\eta t} \hat{S}_\eta^\dagger, \quad (37)$$

in agreement with the results of Josephson and Bardeen<sup>25,26</sup>. When calculating the time evolution it is important to remember that in the lead Hamiltonian the term  $\mu_\eta \hat{N}_\eta$  is still written in terms of electron operators.

Before we proceed, we like to emphasize the importance of the Cooper pair contribution for finite bias voltages. As already pointed out by Governale *et al.*<sup>20</sup>, in this case  $\mu_\eta$  cannot be set to zero and the time evolution of the Cooper pair operators, Eq. (37), plays an important role. Neglecting the Cooper pair contribution for finite bias voltages<sup>35</sup> violates the number conservation in the tunneling processes and can lead to coherences which would vanish in the number conserving case.

#### 2. Difference to the normal conducting theory

To compute Eq. (35) we rewrite the electron operators using the Bogoliubov transformation, Eq. (6), and insert

the time evolution as in Eqs. (36) and (37). This yields four different traces to be calculated. We find:

$$\begin{aligned} \text{Tr}_B \left( \hat{c}_{\eta k \sigma, I}^\dagger(t) \hat{c}_{\eta' k' \sigma', I}(t') \hat{\rho}_B \right) = \\ \delta_{\eta \eta'} \delta_{k k'} \delta_{\sigma \sigma'} \left\{ |u_{\eta k}|^2 f^+(E_{\eta k}) e^{+\frac{i}{\hbar}(E_{\eta k} + \mu_\eta)(t-t')} \right. \\ \left. + |v_{\eta k}|^2 f^-(E_{\eta k}) e^{-\frac{i}{\hbar}(E_{\eta k} - \mu_\eta)(t-t')} \right\}, \end{aligned} \quad (38)$$

$$\begin{aligned} \text{Tr}_B \left( \hat{c}_{\eta k \sigma, I}(t) \hat{c}_{\eta' k' \sigma', I}^\dagger(t') \hat{\rho}_B \right) = \\ \delta_{\eta \eta'} \delta_{k k'} \delta_{\sigma \sigma'} \left\{ |u_{\eta k}|^2 f^-(E_{\eta k}) e^{-\frac{i}{\hbar}(E_{\eta k} + \mu_\eta)(t-t')} \right. \\ \left. + |v_{\eta k}|^2 f^+(E_{\eta k}) e^{+\frac{i}{\hbar}(E_{\eta k} - \mu_\eta)(t-t')} \right\}, \end{aligned} \quad (39)$$

$$\begin{aligned} \text{Tr}_B \left( \hat{c}_{\eta k \sigma, I}^\dagger(t) \hat{c}_{\eta' k' \sigma', I}^\dagger(t') \hat{\rho}_B \right) = \delta_{\eta \eta'} \delta_{k-k'} \delta_{\sigma \bar{\sigma}'} \\ \text{sgn } \sigma \ v_{\eta k}^* u_{\eta k} e^{\frac{i}{\hbar} 2\mu_\eta t} \left\{ f^-(E_{\eta k}) e^{-\frac{i}{\hbar}(E_{\eta k} + \mu_\eta)(t-t')} \right. \\ \left. - f^+(E_{\eta k}) e^{+\frac{i}{\hbar}(E_{\eta k} - \mu_\eta)(t-t')} \right\}, \end{aligned} \quad (40)$$

$$\begin{aligned} \text{Tr}_B \left( \hat{c}_{\eta k \sigma, I}(t) \hat{c}_{\eta' k' \sigma', I}(t') \hat{\rho}_B \right) = \delta_{\eta \eta'} \delta_{k-k'} \delta_{\sigma \bar{\sigma}'} \\ \text{sgn } \sigma \ v_{\eta k} u_{\eta k}^* e^{-\frac{i}{\hbar} 2\mu_\eta t} \left\{ f^+(E_{\eta k}) e^{+\frac{i}{\hbar}(E_{\eta k} + \mu_\eta)(t-t')} \right. \\ \left. - f^-(E_{\eta k}) e^{-\frac{i}{\hbar}(E_{\eta k} - \mu_\eta)(t-t')} \right\}, \end{aligned} \quad (41)$$

where  $f^-(E) = 1 - f^+(E)$ . In contrast to normal conducting theory, the traces of Eqs. (40) and (41) are not vanishing in the superconducting case. However, to second order in perturbation theory they do not contribute to the time evolution of the density matrix, for reasons to be presented later. They are crucial in higher order perturbation theory and yield e.g. the phase-dependent Josephson current<sup>20</sup>.

### B. General Master Equation for the reduced density matrix

Collecting all the previous results and expressing Eq. (35) in the basis of the system eigenstates we obtain the Bloch-Redfield form of the general master equation (GME) for the reduced density matrix:

$$\begin{aligned} \dot{\hat{\rho}}_{nn'} = & -\frac{i}{\hbar} (E_n - E_{n'}) \hat{\rho}_{nn'}(t) \\ & - \sum_{mm'} \left( R_{nn'mm'}^{N \rightarrow N+1} + R_{nn'mm'}^{N \rightarrow N-1} \right. \\ & \left. + Q_{nn'mm'}^{N \rightarrow N+1} + Q_{nn'mm'}^{N \rightarrow N-1} \right) \hat{\rho}_{mm'}(t), \end{aligned} \quad (42)$$



where we defined the Redfield-tensors:

$$R_{nn'mm'}^{N \rightarrow N \pm 1} = \sum_{\eta} \left\{ \delta_{m'n'} \sum_l (\Gamma_{nllm}^+)^{N \rightarrow N \pm 1}_{\eta} + \delta_{mn} \sum_l (\Gamma_{m'ln'}^-)^{N \rightarrow N \pm 1}_{\eta} - (\Gamma_{m'n'nm}^+)^{N \rightarrow N \pm 1}_{\eta} - (\Gamma_{m'n'nm}^-)^{N \rightarrow N \pm 1}_{\eta} \right\}, \quad (43)$$

and

$$Q_{nn'mm'}^{N \rightarrow N \pm 1} = \sum_{\eta} \left\{ \delta_{m'n'} \sum_l (\Sigma_{nllm}^+)^{N \rightarrow N \pm 1}_{\eta} + \delta_{mn} \sum_l (\Sigma_{m'ln'}^-)^{N \rightarrow N \pm 1}_{\eta} - (\Sigma_{m'n'nm}^+)^{N \rightarrow N \pm 1}_{\eta} - (\Sigma_{m'n'nm}^-)^{N \rightarrow N \pm 1}_{\eta} \right\}. \quad (44)$$

In Eqs. (43) and (44) we introduced rates  $\Gamma$ , which we call “normal”, and rates  $\Sigma$ , which we call “anomalous”. The anomalous rates  $\Sigma$  come from terms containing traces of the type of Eqs. (40) and (41). In App. C we show that they are equal to zero. The normal rates originate from terms containing traces of the type of Eqs. (38) and (39). Further, we distinguish between rates describing the increase and rates describing the decrease of the particle number on the system, emphasized with the superscript  $N \rightarrow N \pm 1$ . Their detailed form is presented in App. C. The normal rates with the superscripts  $\pm$  are connected by complex conjugation and reversing of the indices:

$$(\Gamma_{nmm'n'}^-)^{N \rightarrow N \pm 1}_{\eta} = \left( (\Gamma_{n'm'mn}^+)^{N \rightarrow N \pm 1}_{\eta} \right)^*. \quad (45)$$

### C. Current

Having derived the GME for the reduced density matrix in Eq. (42), we can use it to calculate measurable quantities like the current and the differential conductance. In this section we present an expression for the current derived from the second order GME of Eq. (42). To do this we introduce a current operator whose statistical average gives the total current:

$$I_{\eta} = \text{Tr}(\hat{I}_{\eta} \hat{\rho}_{tot}). \quad (46)$$

In general, the current operator of lead  $\eta$  is defined as the variation of the total particle number in lead  $\eta$  with time:

$$\hat{I}_{\eta,I}(t) = -e \frac{d}{dt} \hat{N}_{\eta,I}(t) = \frac{+ie}{\hbar} \left[ \hat{N}_{\eta,I}(t), \hat{H}_{T,I}(t) \right]. \quad (47)$$

Calculating the commutator of Eq. (47), we see that the current operator has the same operatorial structure as the tunneling Hamiltonian:

$$\hat{I}_{\eta,I}(t) = \frac{+ie}{\hbar} \sum_{k\alpha} \left( t_{\eta\alpha\sigma} \hat{c}_{\eta k\sigma,I}^{\dagger}(t) \hat{d}_{\alpha\sigma,I}(t) - t_{\eta\alpha\sigma}^* \hat{d}_{\alpha\sigma,I}^{\dagger}(t) \hat{c}_{\eta k\sigma,I}(t) \right), \quad (48)$$

differing only in the prefactor and summation. Hence, by applying the same perturbation theory as before, we obtain for the current in lead  $\eta$ :

$$I_{\eta}(t) = e \sum_{nml} \left( (\Gamma_{nllm}^{N \rightarrow N+1})_{\eta} - (\Gamma_{nllm}^{N \rightarrow N-1})_{\eta} \right) \rho_{mn}^N(t). \quad (49)$$

In Eq. (49) we introduced the abbreviations

$$\begin{aligned} (\Gamma_{nmm'n'}^{N \rightarrow N \pm 1})_{\eta} &= (\Gamma_{nmm'n'}^+)^{N \rightarrow N \pm 1}_{\eta} + (\Gamma_{nmm'n'}^-)^{N \rightarrow N \pm 1}_{\eta} \\ &= 2 \text{Re} \left( (\Gamma_{nmm'n'}^+)^{N \rightarrow N+1}_{\eta} \right), \end{aligned} \quad (50)$$

exploiting Eq. (45). This gives us rates which are real and read:

$$\begin{aligned} (\Gamma_{nmm'n'}^{N \rightarrow N+1})_{\eta} &= \text{Re} \left( \tilde{\Gamma}_{nmm'n'}^{\eta} D(E_{m'n'} - \mu_{\eta} + i\gamma) \right. \\ &\quad \left. \times f^+(E_{m'n'} - \mu_{\eta} + i\gamma) \right), \end{aligned} \quad (51)$$

$$\begin{aligned} (\Gamma_{nmm'n'}^{N \rightarrow N-1})_{\eta} &= \text{Re} \left( \tilde{\Gamma}_{m'n'nm}^{\eta} D(E_{n'm'} - \mu_{\eta} + i\gamma) \right. \\ &\quad \left. \times f^-(E_{n'm'} - \mu_{\eta} + i\gamma) \right), \end{aligned} \quad (52)$$

where

$$\tilde{\Gamma}_{nmm'n'}^{\eta} = \frac{2\pi}{\hbar} \sum_{\sigma\alpha\alpha'} t_{\eta\alpha\sigma} t_{\eta\alpha'\sigma}^* \langle n | \hat{d}_{\alpha\sigma} | m \rangle \langle m' | \hat{d}_{\alpha'\sigma}^{\dagger} | n' \rangle. \quad (53)$$

In Eqs. (51) and (52)  $E_{n'm'} = E'_n - E'_m$  denote differences between system eigenenergies and

$$D(E) = \rho_N \text{Re} \left( \frac{|E|}{\sqrt{E^2 - |\Delta|^2}} \right), \quad (54)$$

is the BCS-density of states, with  $\rho_N = \frac{Vmk_F}{2\pi^2\hbar^2}$  labeling the density of states for normal leads which is assumed to be constant around the Fermi level;  $V$  denotes the volume of the lead and  $m$  is the electron mass. In order to renormalize the divergence of the density of states we introduced a finite lifetime  $\hbar/\gamma$  of the quasiparticle states in the superconducting leads, leading to a Lorentzian broadening of the resonance condition, see App. C3. This assumption is also in agreement with the results of Levy

Yeyati *et al.*<sup>17</sup>, where they showed that the broadening of the BCS-like features in the current is due to the coupling to the leads. Eq. (49) is a general result and can be applied to any transport set-up where an arbitrary system with discrete levels is weakly coupled to superconducting or normal conducting leads. The normal conducting case is obtained by setting  $|\Delta_\eta| = 0$  and  $\gamma = 0$ .

In this article we are only interested in the stationary limit. Hence, we replace the density matrix in Eq. (49) by its stationary solution which is determined from Eq. (42) by imposing  $\dot{\rho}_{nn'}^N = 0$ .

## V. TRANSPORT THROUGH MULTIPLE QUANTUM DOT DEVICES

In the preceding sections we developed a perturbative microscopic theory for the stationary current of quantum dot devices coupled to superconducting leads. In the following, we show the predictions of the theory for two models, the single level quantum dot (SD) and the double quantum dot (DD). In the transport set-up the bias and gate voltages influence the energy configuration of the leads and the system, respectively. Specifically, the bias voltage is modifying the electrochemical potential of the leads, which we choose to have a symmetric voltage drop. Therefore we define the chemical potentials of the left and right lead, respectively:

$$\mu_{L/R} = \mu_0 \pm e \frac{V_b}{2}, \quad (55)$$

where  $\mu_0$  is the equilibrium chemical potential. The gate voltages are modifying the on site energies of the system: we replace  $\epsilon_d \rightarrow \epsilon_d + eV_g$  in the SD- and  $\epsilon_\alpha \rightarrow \epsilon_\alpha + eV_g^\alpha$  in the DD-Hamiltonian. Here  $e = -|e|$  is the electron charge.

In the following we neglect coherences in the GME, considering only diagonal contributions of the reduced density matrix  $\rho_{nn}$  by setting  $n = n'$  in Eq. (42). Hence, it suffices to use only two indices for the transition rates.

In current voltage spectroscopy it is convenient to illustrate the conditions under which current is allowed to flow as lines in the stability diagrams. These so called transition lines are fixed by the energetic part of the transition rates at the source  $\eta = S$  and the drain  $\eta = D$  contact:

$$(\Gamma_{mn}^{N \rightarrow N+1})_\eta \propto f^+(\Delta E - \mu_\eta) D(\Delta E - \mu_\eta), \quad (56)$$

$$(\Gamma_{nm}^{N+1 \rightarrow N})_\eta \propto f^-(\Delta E - \mu_\eta) D(\Delta E - \mu_\eta), \quad (57)$$

neglecting the lifetime broadening  $\gamma$  for simplicity, and with  $\Delta E = E_m^{N+1} - E_n^N$  the energy difference of the two transport levels. Fig. 2 illustrates this product for two different temperatures: for high enough temperatures quasiparticles can be excited thermally across the gap giving a small peak in the transition rates<sup>16</sup>. The peak

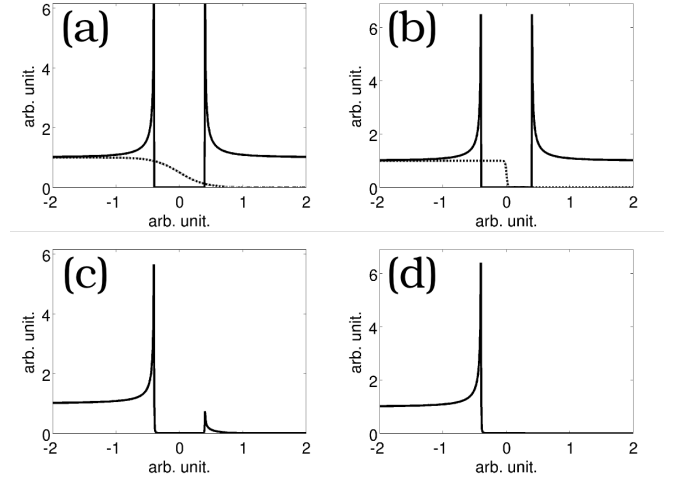


Figure 2. Panels (a) and (b): Density of states (continuous line) and Fermi function (dotted line) at  $k_B T = 0.2$  meV and  $k_B T = 0.01$  meV, respectively. Panels (c) and (d): Product of the density of states and the Fermi function for the temperatures used in Fig. (a) and (b), respectively.

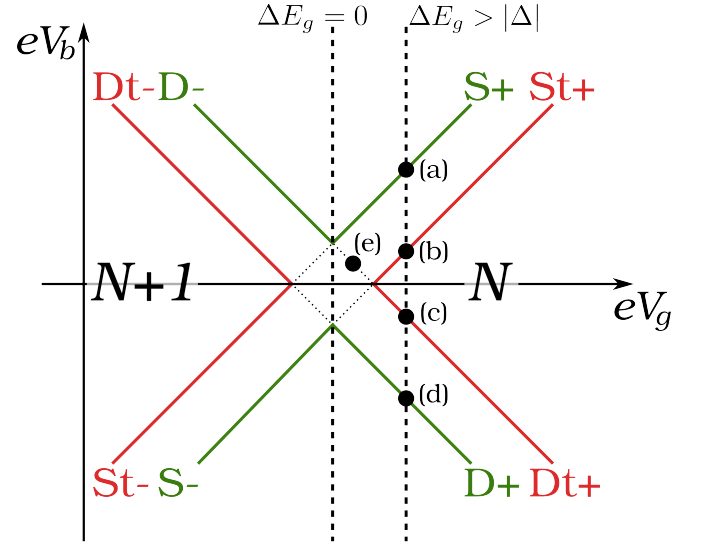


Figure 3. (Color online) Illustration of the transition lines appearing in presence of superconducting leads. The green lines mark transitions at the **S**ource and the **D**rain contacts, described by the inequalities of Eqs. (58), (59), (62), and (63). The red lines mark transitions involving thermally excited quasiparticles, given by Eqs. (60), (61), (64), and (65). The  $E_g$ - $N$  diagrams for the points (a)-(e) are sketched in Fig. 5.

positions define transition lines when plotted in a  $V_g$ - $V_b$  diagram. Notice that while the most pronounced peak survives also at zero temperature and defines a transport threshold, the second peak vanishes at low temperatures and essentially only processes at and close to the peak are relevant. For an  $N \rightarrow N + 1$  transition we denote transitions associated to the more pronounced peak as S+ and D+ when happening at the source or at the drain

contact, respectively. Transitions involving thermally excited quasiparticles are called St+ and Dt+. In complete analogy, we classify transitions from  $N + 1 \rightarrow N$ : we denote by S- and D- the more pronounced transitions at the source and at the drain, and by St- and Dt- their thermal counterparts. In total we find 8 different transition lines, as depicted in Fig. 3. In the following we derive transport conditions and provide equations for the transport lines. For convenience we introduce  $\Delta E_g = \Delta E - \mu_0$ .

We start with the analysis of the  $N \rightarrow N + 1$  transitions, which are described by the rates in Eq. (56). From the arguments we find that the rates do not vanish if

**Source S+:**

$$\Delta E_g \leq -|\Delta| + \frac{eV_b}{2} \Rightarrow \frac{eV_b}{2} \geq \Delta E_g + |\Delta|, \quad (58)$$

**Drain D+:**

$$\Delta E_g \leq -|\Delta| - \frac{eV_b}{2} \Rightarrow \frac{eV_b}{2} \leq -\Delta E_g - |\Delta|. \quad (59)$$

Another contribution comes from the thermally excited quasiparticles states, namely, if the argument of the Fermi function  $f^+(\Delta E - \mu_\eta)$  and of the density of states  $D(\Delta E - \mu_\eta)$  is equal to  $|\Delta|$ . At this point the transition rates are peaked and contribute to the current:

**Source (thermal) St+:**

$$\Delta E_g = |\Delta| + \frac{eV_b}{2} \Rightarrow \frac{eV_b}{2} = \Delta E_g - |\Delta|, \quad (60)$$

**Drain (thermal) Dt+:**

$$\Delta E_g = |\Delta| - \frac{eV_b}{2} \Rightarrow \frac{eV_b}{2} = -\Delta E_g + |\Delta|. \quad (61)$$

Since the thermally excited quasiparticles produce a peak rather than a step in the current voltage characteristic, the corresponding transport condition is formulated with an equality.

Transitions from  $N + 1 \rightarrow N$  are described by the rate of Eq. (57), leading in complete analogy to the previous case to the following transport conditions:

**Source S-:**

$$-\Delta E_g \leq -|\Delta| - \frac{eV_b}{2} \Rightarrow \frac{eV_b}{2} \leq \Delta E_g - |\Delta|, \quad (62)$$

**Drain D-:**

$$-\Delta E_g \leq -|\Delta| + \frac{eV_b}{2} \Rightarrow \frac{eV_b}{2} \geq -\Delta E_g + |\Delta|, \quad (63)$$

**Source (thermal) St-:**

$$-\Delta E_g = |\Delta| - \frac{eV_b}{2} \Rightarrow \frac{eV_b}{2} = \Delta E_g + |\Delta|, \quad (64)$$

**Drain (thermal) Dt-:**

$$-\Delta E_g = |\Delta| + \frac{eV_b}{2} \Rightarrow \frac{eV_b}{2} = -\Delta E_g - |\Delta|. \quad (65)$$

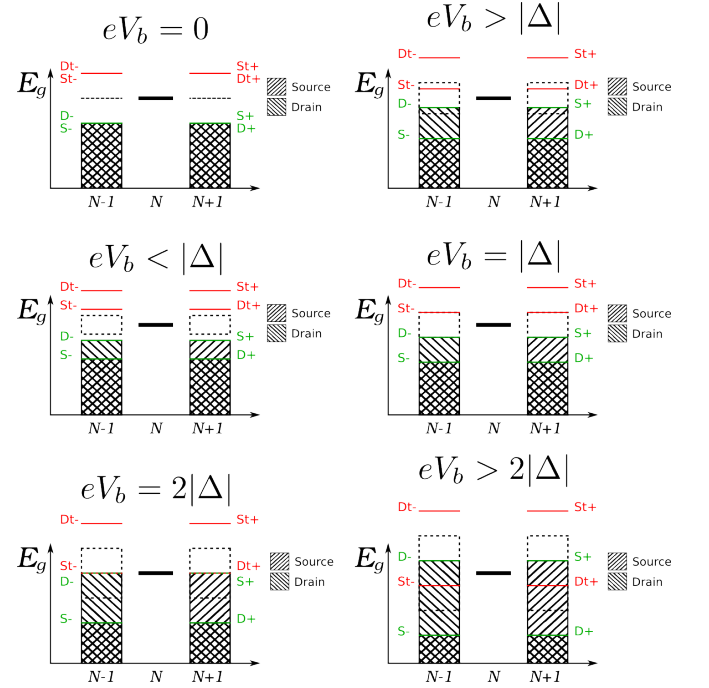


Figure 4. (Color online) Visualization of the transport conditions of Eqs. (58)-(65). We plotted the threshold of the transport inequalities as green lines (S $\pm$ , D $\pm$ ); for the equalities coming from transitions involving thermally excited quasiparticles we used red lines (St $\pm$ , Dt $\pm$ ). Choosing the reference level in the  $N$  particle subspace, we found a scheme where transitions are energetically allowed to levels which lie in the shaded region below the green lines and to levels which align with the red lines. The dashed box marks the bias window  $eV_b$ .

### 1. Visualization of the transport conditions

To visualize the transport conditions of Eqs. (58)-(65) we extend the scheme of Donarini *et al.* of Ref. 36 to superconducting leads. The scheme is depicted in Fig. 4 and illustrates for which relative position of the systems eigenenergies  $E_g^N = E_m^N - \mu_0 N$  transitions are energetically allowed. The green lines mark the borders of the inequalities, the red lines the sharp equalities for the thermal transitions, meaning that transitions can occur to states lying below the green lines, and to states which coincide with the red lines. In order to see a transition between two levels in the stability diagram a source and a drain transition must be allowed between the two levels (depicted as arrows in the  $E_g$ - $N$  diagrams of Fig. 5). We note that for a full analysis of the transport properties also the geometrical part of the rates must be taken into account and transport occurs only if  $\tilde{\Gamma} \neq 0$ .

### A. Single level quantum dot model

The simplest example of a quantum dot system is the single level quantum dot presented in Eq. (2). Since only



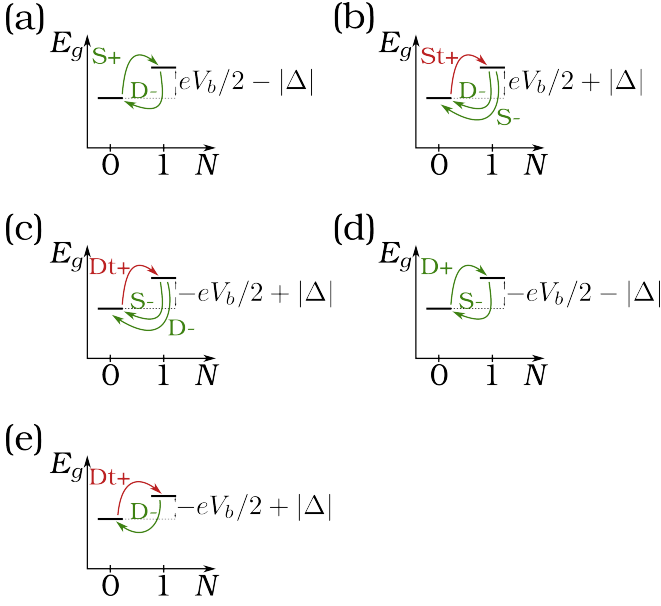


Figure 5. (Color online) (a)-(d):  $E_g$ - $N$  diagrams for a single level quantum dot with  $\Delta E_g > |\Delta|$  and at bias voltages as sketched in Fig. 3. For the simulations of Fig. 6  $\Delta E_g > \Delta$  corresponds to a gate voltage  $eV_g < -2.6$  meV. In (a) we cut the S+ line: the particle number on the system is increased by a tunneling event at the source contact and decreased at the drain. (b) Cut with the thermal line St+: the particle number of the system is increased by a tunneling event involving a thermally excited quasiparticle at the source contact and decreased by tunneling into empty states in the source drain, respectively. Increasing further the bias voltage until its sign changes leads to an interchange of the role of the source and the drain voltage. Hence, (c) and (d) describe the same situation as (a) and (b) under  $S \leftrightarrow D$ . (e):  $E_g$ - $N$  diagrams for a single level with  $0 < \Delta E_g < |\Delta|$ . The two levels are only connected by two drain transitions, meaning that in this configuration the system is in thermal equilibrium with the drain contact.

one level is involved, we can do most calculations analytically and understand the basic mechanism resulting from the superconducting leads. In Fig. 6 the stationary current is shown as a function of bias and gate voltage for superconducting leads at  $k_B T = 0.5|\Delta|$ . We observe the expected gap<sup>5</sup> between the Coulomb diamonds which is equal to  $4|\Delta|/e$ . The gap can be explained using Fig. 3 and the corresponding Eqs. (58)-(65). One dashed line marks the gate voltage where  $\Delta E_g = 0$ . Along this line the conditions under which current is allowed to flow read:  $eV_b/2 > |\Delta|$  for the S+, D- lines, and  $eV_b/2 < -|\Delta|$  for the S-, D+ lines, opening a bias window of  $4|\Delta|/e$  where current is blocked for low temperatures  $k_B T \ll |\Delta|$ . For higher temperatures of  $k_B T \approx 0.5|\Delta|$  we observe small peaks in the Coulomb blockade region (green area) which are due to thermally excited quasiparticles, they correspond to the red lines in Fig. 3. In Fig. 5 we show the energy particle number diagrams in the points (a)-(d), which lie on a vertical cut through

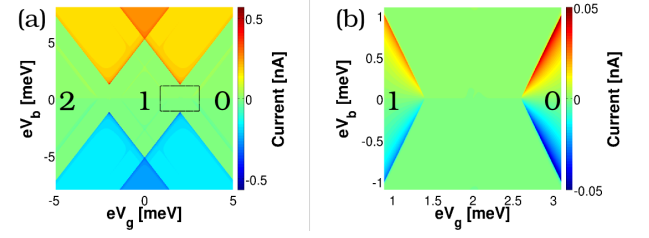


Figure 6. (Color online) (a) Current voltage characteristics of a SD coupled to superconducting leads. Parameters are  $k_B T = 0.3$  eV and  $|\Delta| = 0.6$  meV. (b) Subgap features coming from thermally excited quasiparticles of the 0-1-particle transition, highlighted as a dashed box in (a).

Fig. 3 at  $\Delta E_g > |\Delta|$  which corresponds to a gate voltage  $eV_g > 2.6$  meV in Fig. 6. In Fig 5 (a) we depicted the  $E_g$ - $N$  diagram for a cut with the S+ resonance line, where the particle number on the system is increased by a tunneling event at the source and decreased at the drain contact. For bias voltages smaller than the one at resonance (corresponding to larger  $eV_b$  as  $e$  is the negative charge of an electron) the S+, D- transitions remain open and current can flow. In Fig. 5 (b) the  $E_g$ - $N$  diagram at the resonance line St+ is shown. In this case the bias voltage is not large enough to allow the transitions S+ of Eq. (58). For low temperatures no quasi particle is thermally excited meaning that only transitions from  $1 \rightarrow 0$  are energetically allowed (green arrows). For high enough temperatures, however, the particle number of the system can be increased by tunneling events involving thermally excited quasiparticles opening the St+ transition. By changing the sign of the bias voltage the role of the source and the drain is inverted, explaining the transition lines Dt+ and Dt (Fig. 5 (c) and (d)).

Another interesting constellation of the energy level occurs in the region of  $0 < \Delta E_g < |\Delta|$  (Fig. 5 (e)), where in the current-voltage characteristics the thermal lines are vanishing. Transitions can only occur at the drain contact, as the bias is not large enough to allow transitions at the source. Hence, the system is in thermal equilibrium with the drain contact and the occupation probabilities are related by the Boltzmann distribution:

$$\frac{\rho_0}{\rho_1} = e^{\beta(\Delta E_g + eV_b/2)}, \quad (66)$$

in the limit of  $\gamma \rightarrow 0$ .

## B. The double quantum dot

We have seen that the theory can reproduce well known results for the SD and we understood the properties of the thermal transitions in  $E_g$ - $N$  diagrams with only one non degenerated level per particle number. In the following we investigate a more advanced system, the double quantum dot, where the many body spectrum gives

rise to more than one non degenerated level per particle number, so called excited system states. For normal conducting leads the excitations cannot be seen for low bias voltages, since transitions to the ground state are always possible, blocking transport through the excitations. In the last subsection we have seen that for superconducting leads the energy difference must be at least  $|\Delta E_g| \geq eV_b/2 - |\Delta|$  to have non thermal source and drain transitions. Hence, we find situations where the transition to the ground state are energetically not allowed and transport occurs through excited system states.

We start with equally gated dots with the same on-site energies and on-site Coulomb interactions, where it is possible to diagonalize the Hamiltonian analytically<sup>30,31</sup>. In the second part, the case of independently coupled dots is discussed, where the detuning of the two gate voltages influences the level spacing of the energy spectrum. Thus, excited states can be observed only in detuning ranges where the difference between the energy level of the excited state and its ground state is less than  $2|\Delta|$ .

### 1. Equally gated dots

For equally gated dots the on-site energies of the two sites are modulated with the same gate voltage. Hence, it is convenient to plot the current as a function of the bias and the gate voltage as for the SD. Fig. 7 shows the current of an equally gated DD in serial configuration. As for the SD we observe Coulomb blockade and the gap of  $4|\Delta|/e$  between the tips of the diamonds. Transport carried by thermally excited quasiparticles is of particular interest, as it allows to observe transitions through excited system states for low bias voltages, which are often diminished by the ground state transitions in the normal conducting case. In order to show some interesting phenomena resulting from the more complex spectrum, we concentrate on the 0- to 1-particle transition where three levels are involved. In the 1-particle spectrum, the difference between the ground state and the excited state is equal to  $2|b|$ , where  $b < 0$  is the tunneling strength between the two dots. Meaning that by tuning the coupling between the two dots it is possible to influence the level spacing. Fig. 8 shows a sketch of the transition lines expected for the 0 – 1 transition for  $|b| < |\Delta|$ , where the red (green) lines show the ground state to ground state transitions, and the blue (orange) lines the ground state to first excited state transitions. For a better understanding of the transport properties we cut the transitions lines horizontally for a small bias voltage  $eV_b/2 < |\Delta|$  in the Coulomb blockade region (points (A)-(D)), the corresponding  $E_g$ - $N$  diagrams are depicted in Fig. 9. In point (A) the difference between the ground states is equal to  $\Delta E_g = eV_b/2 + |\Delta|$  opening the thermal transition  $St+$  and current can flow. Following the dashed line to point (B), the 1 particle states are shifted down in energy until the  $St+$  transition is allowed between the 0-particle ground state and the 1-particle ex-

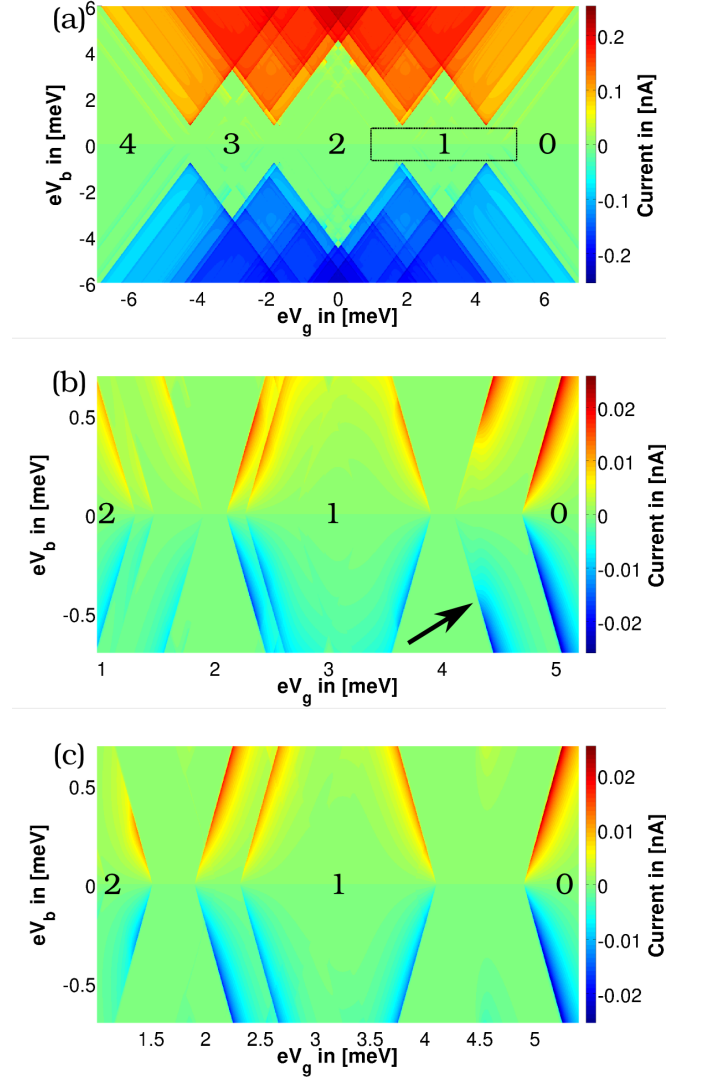


Figure 7. (Color online) (a) Current voltage characteristics of an equally gated DD in serial configuration at  $k_B T = 0.2$  meV and  $|\Delta| = 0.4$  meV. (b) I-V characteristics in the subgap region corresponding to the dashed box in (a). The distance between the 1-particle excited state and its ground state is equal to the coupling strength  $2|b|$  of the two dots. Moreover,  $2|b| < 2|\Delta|$ . The black arrow marks the transition line coming from transport through the 1-particle excited state. (c) I-V-characteristics in the subgap region, where we increased the coupling between the two dots, leading to a level spacing which is larger than  $2|\Delta|$ , hence transport through the excited system state is not allowed and the line disappears.

cited state. Since  $|b| < \Delta$ , the 1-particle ground state is energetically not accessible and current can flow through the excited state. We like to emphasize that the blocking of the ground state transition is only valid as long as the distance between the two 1-particle levels is smaller than  $2|\Delta|$ . For larger distances the ground state is energetically accessible, blocking the current through the excited state, c.f. Fig. 10. In point (C)  $eV_g$  is further decreased,

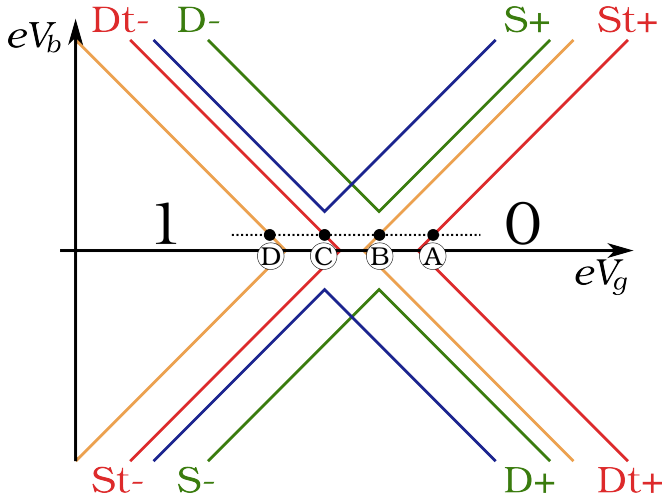


Figure 8. (Color online) Sketch of the transition lines for the 0-1 particle transition of an equally gated DD. It shows two copies of Fig. 3 where the labeling of the blue (orange lines) is the same as for the green (red) lines. The blue (orange) lines mark the transition lines corresponding to the 0- particle ground state to 1-particle first excited state transition.

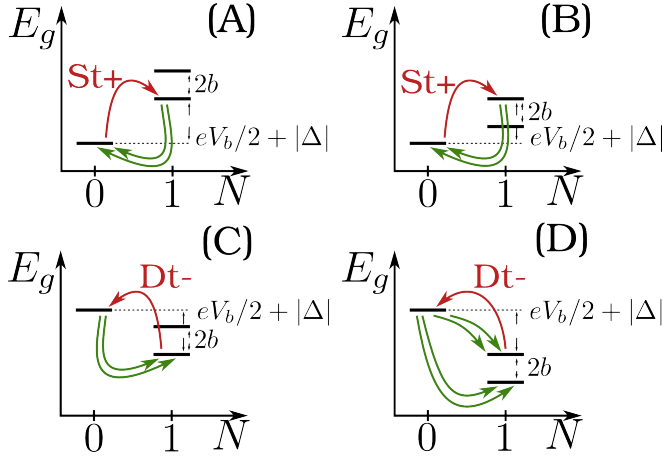


Figure 9. (Color online)  $E_g$ - $N$  diagram corresponding to the points of Fig. 8 where the dashed line cuts the transition lines for the case of an equally gated DD. In this case the distance between the 1-particle ground state to the 1-particle first excited state is equal to  $2b < 2|\Delta|$ , where  $b$  is the tunneling strength between the two quantum dots. (A) Point on the thermal line St+ of the ground state to ground state transition. (B) Point on the thermal line St+ of the ground state to first excited state transition. (C) Point on the Dt- line of the ground state to ground state transition. (D) Point on the Dt- line of the ground state to first excited state transition; this line cannot be seen in the current voltage characteristics, as the ground state to ground state transitions are open. Hence, in the long time behavior the system will occupy the 1-particle ground state blocking the current through the excited state.

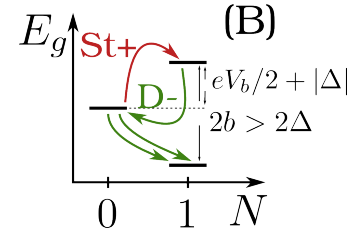


Figure 10. (Color online)  $E_g$ - $N$  diagram of point (B) in Fig. 8, for a level spacing of the one particle energies larger than  $2b > 2\Delta$ . In contrast to Fig. 9 the transition between the 0-particle ground state and the 1-particle excited state is open, blocking the current.

the Dt- transition between the ground states is opening, and current can flow. Point (D) shows the typical energy configuration in which current through the excited state is blocked, even though the transition through the excited state is energetically allowed. The reason for that is the 1-particle ground state which can be populated, but transitions describing its depopulation are energetically not allowed, leading to a blocking of the current in the stationary limit.

To demonstrate the important role of the level spacing we show the current voltage characteristics of an equally gated DD in the subgap region in Fig. 7 (b-c). In (b) the spacing of the 1-particle energy levels  $|2b| < 2|\Delta|$ , hence, the excited state can be observed in the current (arrow in Fig. 7). In (c) we increase the tunneling strength between the two dots  $2|b| > 2|\Delta|$  and the excited state line is vanishing, as explained in Fig. 10. As in the case for  $2|b| < 2|\Delta|$  the excited level is in resonance with the St+ transition, however, due to the larger level spacing, the ground state transition opens and current is blocked.

## 2. Independently gated dots

In the last paragraph we considered a DD with both dots coupled to the same gate electrode. In most experiments, however, it is more convenient to couple the dots independently, which leads to a 'honeycomb' shaped current voltage characteristics<sup>37</sup>. For symmetric on-site energies and Coulomb repulsion it is possible to diagonalize the DD Hamiltonian of Eq. (3) analytically. Gating the dots independently destroys this symmetry, an analytically diagonalization is not possible, and one has to use numerical methods. We plot the current as a function of the detuning  $\Delta_g = V_g^1 - V_g^2$ , and the average of the two gate voltages  $\Sigma_g = (V_g^1 + V_g^2)/2$ .

The current voltage characteristic for serial and parallel configuration is depicted for the normal conducting case in Fig. 11 (a)-(b) and for the superconducting case in Fig. 11 (c)-(d). Comparing both configurations, we observe for the serial one a decrease in the current for high detuning  $\Delta_g$ , while in the parallel configuration current can be observed over the entire voltage range. This

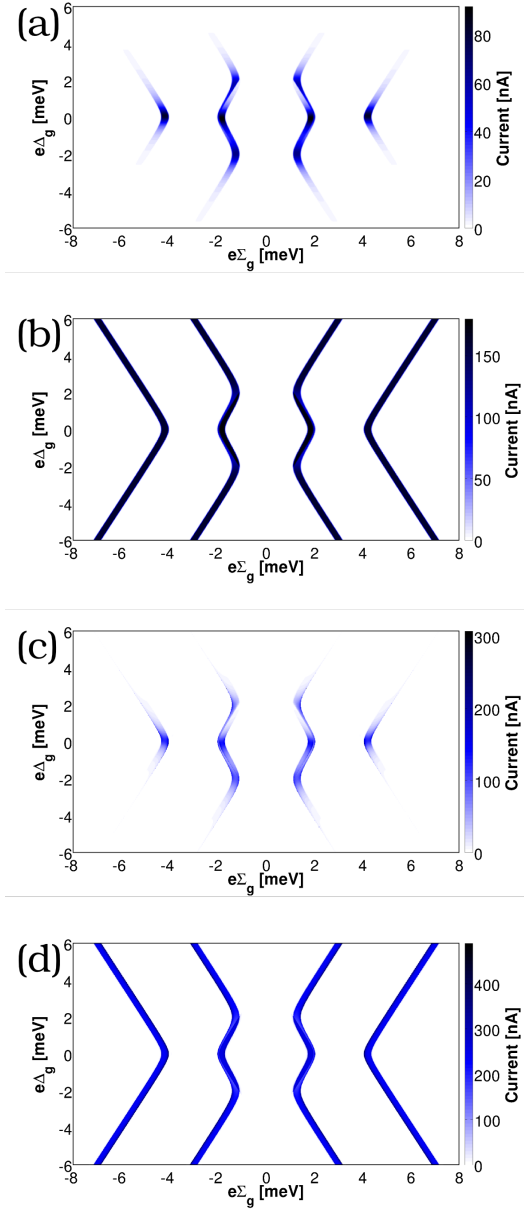


Figure 11. (Color online) (a)-(b) Current voltage characteristics of a DD coupled to normal conducting leads in serial (a) and in parallel (b) configuration. We fixed the bias voltage to  $eV_b = 0.3$  meV. (c)-(d) Current voltage characteristics of a DD coupled to superconducting leads in serial (c) and in parallel (d) configuration. We fixed the bias voltage to  $eV_b = 0.3$  meV +  $2|\Delta|$  in order to obtain the same conditions as for the normal conducting case in (a)-(b).

difference is a consequence of the geometry of the set-up as the DD system remains unchanged. An increase of the detuning leads to a localization of the systems ground state at site 1 and transitions through site 2 are blocked. Since in serial configuration the right lead is only coupled to site 2, the localization of the wave function at site 1 leads to a decrease in the current. In parallel configuration, however, both sites are coupled to both leads and

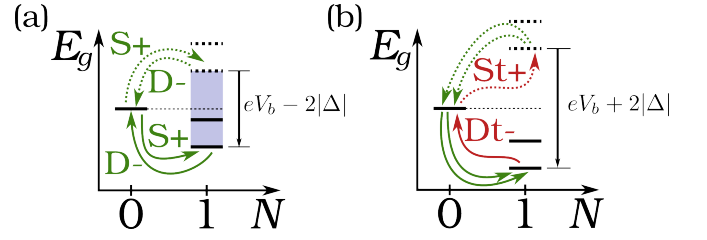


Figure 12. (Color online) (a)  $E_g$ - $N$  diagram of the 0-1-particle transition for  $eV_b/2 > |\Delta|$ . In the 1-particle spectrum we plotted two situations which mark the borders of the current step. The dashed levels mark the left border (for small  $\Sigma_g$ ) where the 1-particle levels lie above the 0-particle energy level. If the distance  $\Delta E_g \leq eV_b/2 - |\Delta|$  current can flow through S+ and D- transitions. By lowering  $e\Sigma_g$  the 1-particle energy levels move down in the  $E_g$ - $N$  diagram, while the transitions remain open. The solid lines mark the right border of the current steps, as for levels lying below the solid line the D- transition is closed and current is blocked. Thus, the width of the current steps in the current voltage characteristics is:  $e\Delta\Sigma_g = eV_b - 2|\Delta|$ . (b)  $E_g$ - $N$  diagram of the 0-1-particle transition involving thermal transitions. For the same arguments as in (a), the distance between two thermal lines in the current voltage characteristics is equal to  $e\Delta\Sigma_g = eV_b + 2|\Delta|$ .

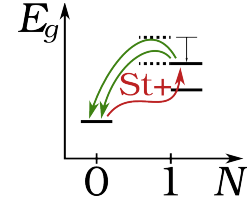


Figure 13. (Color online)  $E_g$ - $N$  diagram for the 0-1-particle transition. Transitions between the two 1-particle levels (dashed lines) and the 0-particle ground state are allowed through the thermal St+ transition. Increasing the gate voltage the levels move down in energy (solid lines) and the excited state transition can be observed when the excited level aligns with the St+ transition. Hence, the distance of two neighboring thermal transitions is equal to the level spacing.

the ground state transition is always open.

The left and right border of the current steps are given by the source and drain lines, respectively. They follow, in complete analogy to the simplest case, from energy conservation. In Fig. 12 (a) we show the  $E_g$ - $N$  diagram for the 0 to 1-particle transition illustrating two limits: the ground states are (i) in resonance with the S+ transition (dashed line) and (ii) in resonance with the D- transition (solid line), describing the left and right borders of the current step in Fig. 11 (c-d). Starting at the S+ resonance, the energy levels of the 1-particle spectrum are moving down in energy by increasing the average gate voltage  $\Sigma_g$ . Both transitions (S+ and D-) remain open as long as the ground state lies in the blue (shaded) region. If the ground state lies below the solid line, the D- transition is closed and current is blocked. Hence, the width of



the current steps in the current voltage characteristics in Fig. 11 (c-d) is equal to the size of the blue (shaded) region in Fig. 12 (a), namely  $e\Delta\Sigma_g = eV_b - 2|\Delta|$ . The same arguments hold for the distance of two corresponding thermal transitions, as illustrated in Fig. 12 (b) the distance of two thermal lines is equal to  $e\Delta\Sigma_g = eV_b + 2|\Delta|$ .

As we can see in Fig. 11 there exists a one to one correspondence of the transport conditions of the normal conducting to the superconducting case which leads to the same shape of the current voltage characteristics if  $k_B T \ll |\Delta|$ . Increasing the bias voltage by  $2|\Delta|$  compared to the normal conducting case  $eV_b^{\text{SC}} = eV_b^{\text{NC}} + 2|\Delta|$  leads to the same transport conditions. Although the shape of the current steps in Figs. 11 (a-b) and 11 (c-d) look the same, they differ at the edges of the current steps, as in the superconducting case the sharp peaks of the quasiparticle density of states are reflected in the current.

### 3. Thermal effects

We have seen that the shape of the stability diagram can be explained using energy conservation, in complete analogy to the simplest case. In this subsection we like to discuss the case for small bias voltages  $eV_b/2 < |\Delta|$ , where current can flow due to thermally excited quasiparticles exclusively. As already observed above, thermally excited quasiparticles do not produce steps in the current voltage characteristics rather they appear as small peaks. This can be used to resolve transitions through excited system states whose energy difference to the ground state is less than  $2|\Delta|$ . By detuning the gate voltages of the two sites of the DD we can change the level spacing of the systems eigenenergies; hence, the excited states are only observed in a certain detuning range. To analyze transitions through excited system states, c.f. Fig. 14, we choose the parallel configuration to rule out the geometrical effect also leading to a decrease of the current for high detuning. If a line corresponding to an excited state disappears for higher detuning  $\Delta_g$ , we conclude that the energy difference to its ground state is larger than  $2|\Delta|$ . In Fig. 15 we plotted the energy differences of the excited states with respect to their ground state for different values of the detuning  $\Delta_g$ , which are marked as red lines in Fig. 14. Counting the number of levels lying under the red line in Fig. 15 gives information about the number of visible excited lines. For instance, consider the case of  $\Delta_g = 0$  in Fig. 15. Following the red line from small to high  $\Sigma_g$  in Fig. 14, we cross the 0-1 particle transitions and observe three lines: two corresponding to the ground state, and one line in between corresponds to a transition through the 1-particle excited state. The distance between the leftmost ground state transition line and the excited line determines the level spacing of the one particle spectrum, see 13. In the 2-particle spectrum the energy difference of one excited state lies under the red line. Hence we should see two lines coming from ex-

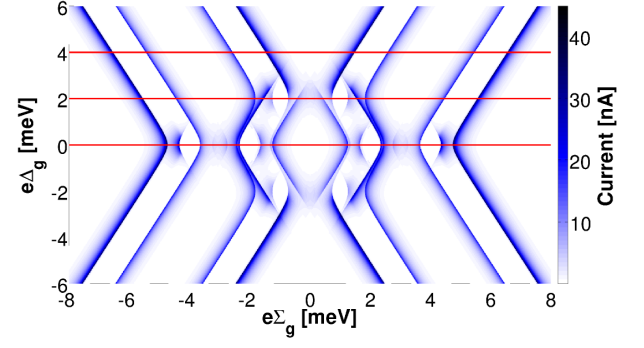


Figure 14. (Color online) Current voltage characteristics of a DD in parallel configuration for bias  $V_b < 2|\Delta|/e$ . Since the bias voltage is not high enough current can flow only due to thermally excited quasiparticles. The red lines correspond to Fig. 15 where the energy differences of the excited states with respect to their ground state are plotted as a function of particle number. The number of visible excited states is proportional to the number of energy differences which are smaller than  $2|\Delta|$  (red line in Fig. 15).

cited system states, namely the transition between the 1-particle ground state and the 2-particle excited state, and transitions between the 2-particle ground state and the 1-particle excited state. Along the horizontal cut at  $\Delta_g = 2$  in Fig. 14, excited states can only be observed for the 1-2 particle and the 2-3 particle transition. This is in agreement with Fig. 15, where only in the 2 particle subspace energy differences lie under the threshold of  $2|\Delta|$ . For higher detuning, e.g.  $\Delta_g = 4$ , no excited states can be seen, as the detuning increases the level spacing, and all energy differences are larger than  $2|\Delta|$  Fig. 15.

### C. The N-QD-S junction

We like to close this article by investigating a so called N-QD-S hybrid system, where a quantum dot system is coupled to a normal and to a superconducting lead, giving a possible explanation for the subgap features in Ref. 1. In the experiment of Ref. 1 a carbon nanotube was contacted to two normal conducting leads and to a superconducting finger in between. The differential conductance between the superconducting finger and a normal lead is measured, realizing a N-QD-S hybrid system. It is possible to apply a bias voltage across the entire tube as well as between the superconductor and a normal conducting lead. The stability diagram in Fig. 2 (a) in Ref. 1, with no bias applied over the entire tube, reveals the typical Coulomb diamond pattern resulting from quasiparticle tunneling with no subgap features. By applying a bias voltage  $V_{SD}$  over the entire tube, the gap in the stability diagram gets smaller with respect to the unbiased case and conductance lines can be seen in the Coulomb blockade region, c.f. Fig. 3 (a) of Ref. 1. The reduction of the gap in the stability diagram is proportional to the



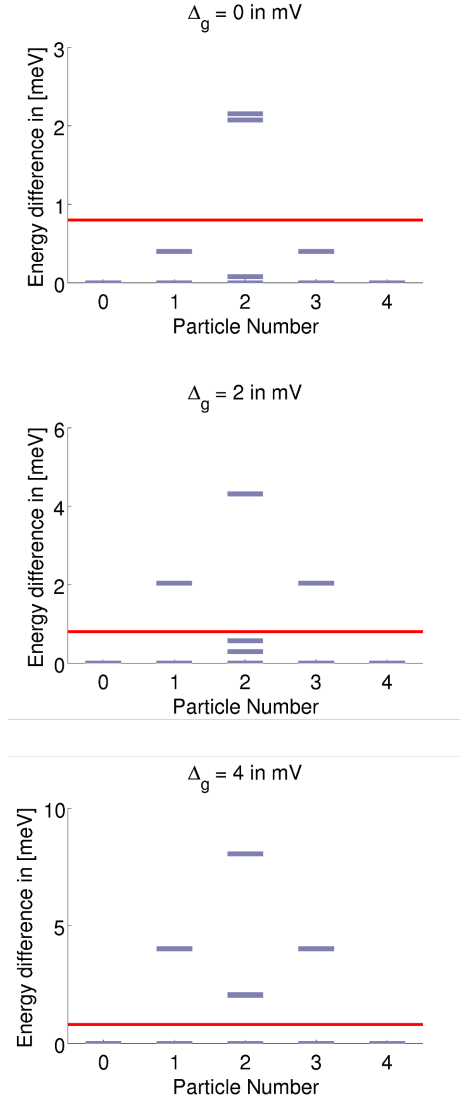


Figure 15. (Color online) Plot of the energy differences of the excited system states with respect to their ground state as a function of particle number. If the energy difference is smaller than  $2|\Delta|$ , transitions through these excited states can be seen in the current voltage characteristics. The threshold of  $2|\Delta|$  is marked as a red horizontal line. We depicted the plots for three situations differing in the detuning  $\Delta_g$ . The three cases are marked as horizontal lines in Fig. 14.

applied bias voltage of approximately  $eV_{SD} \approx |\Delta|/2$ , and is related to an effective reduction of the superconducting gap. For a smaller gap quasiparticles can get thermally excited across the gap leading to subgap transport in complete analogy to the S-QD-S case discussed above.

We can model the N-QD-S system by setting  $|\Delta_S| = 0$  for the normal conducting lead (source) in the master equation; the drain contact remains superconducting  $|\Delta_D| = |\Delta|$ . Hence, the transport conditions change slightly and can be summarized in the scheme of Fig. 18. In Fig. 16 we schematically sketched the expected transition lines for a N-QD-S hybrid structure. In Fig.

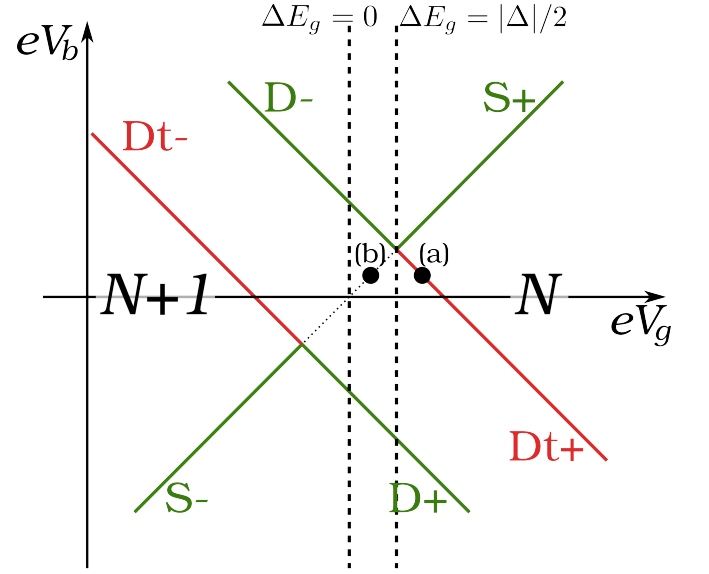


Figure 16. (Color online) Sketch of the transition line of a QD coupled to a normal conducting (source) and a superconducting lead (drain). The difference to the S-QD-S system is that only the drain lines split due to the superconducting gap, the S+ and S- lines are described by the same equation. In this case a gap equal to  $|\Delta|$  is opening, and the triangles are shifted apart. Thermal lines can be observed only for the drain.

19 we analyzed the two most important cases, marked as points (a) and (b) in Fig. 16. Point (a) shows a paradoxical situation as the particle number of the system seems to be increased only at the drain contact, which would lead to a negative current at positive bias. However, if the two contacts have the same temperature, the thermal broadening of the S+ line gives a small contribution in the transition rates (dashed green arrow in Fig. 19 (a)) making the current positive. The situation in (b) shows again the system being in thermal equilibrium with the source contact.

We can see that the lines with negative slope (drain lines) give a finite current in the Coulomb blockade region as observed in Fig. 3 (b) in the experiments. Thus, we claim that the subgap features observed in the experiments possibly are transitions involving thermally excited quasiparticles which are allowed due to the reduction of the superconducting gap. This argument is supported by the observation that for diamonds where the gap has the same size as before (edges of the stability diagram), no subgap lines can be observed. In Fig. 17 we show two  $dI/dV$ -characteristic of a N-QD-S system corresponding to different superconducting gaps with the same temperature ( $k_B T = 0.1 \text{ meV}$ ) in both cases. In (b) the superconducting gap ( $|\Delta| = 0.3 \text{ meV}$ ) is only half of the gap in (a) ( $k_B T = 0.6 \text{ meV}$ ). By reducing the gap, the temperature becomes large enough to excite quasiparticles across the gap, leading to conductance peaks in the Coulomb blockade region, as observed in the experiments. However, a more complex modeling of the multi-terminal

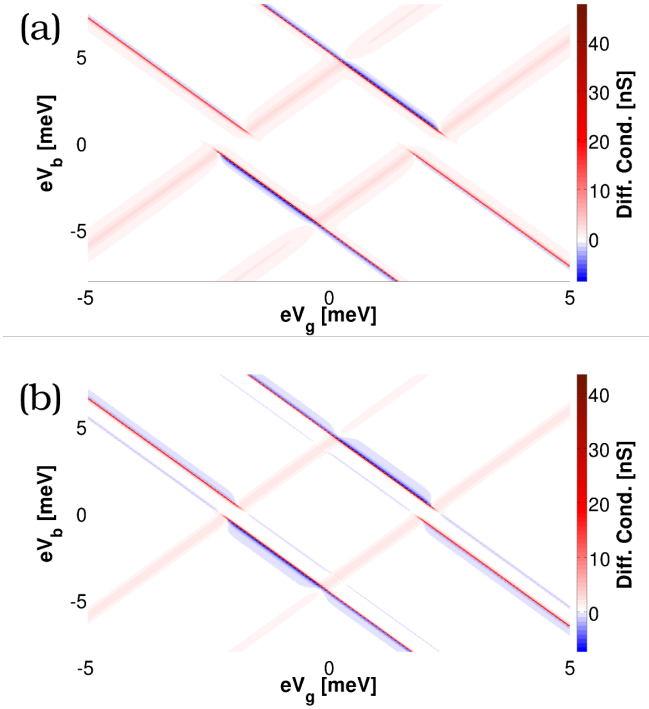


Figure 17. (Color online) Differential Conductance of a SD coupled to a normal conducting (source) and to a superconducting lead (drain) (N-QD-S system). The coupling to the lead is  $e\Gamma = 0.01$  meV. (a) Superconducting gap of  $|\Delta| = 0.6$  meV and temperature  $k_B T = 0.1$  meV. No thermal lines in the subgap region are visible. (b) The same temperature  $k_B T = 0.1$  meV, but for smaller gap  $|\Delta| = 0.3$  meV; quasiparticles get thermally excited across the gap leading to transport in the Coulomb blockade region.

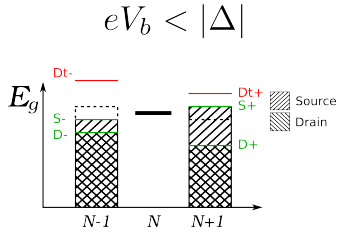


Figure 18. (Color online) Visualization of the transport conditions for a N-QD-S system with  $eV_b/2 < |\Delta|$ , where the source is a normal and the drain a superconducting lead. They follow from Eqs. (58)-(65) by setting  $|\Delta| = 0$  in the equations corresponding to the source lead.

system is required to understand the experiments in all details.

## VI. CONCLUSION

In this work we developed a transport theory for nanostructures coupled to superconducting leads up to second order in the tunneling Hamiltonian. We used the Bo-

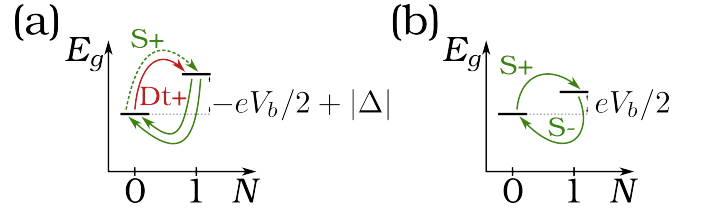


Figure 19.  $E_g$ - $N$  diagrams corresponding to points (a) and (b) of Fig. 16. (a) We see a positive current in the subgap region, which comes only due to the thermal smearing of the  $S+$  transition. (b) The line connecting the  $S+$  and the  $S-$  transition line in the Coulomb blockade region the system is in thermal equilibrium with the source contact.

goliubov transformation to describe the electrons in the superconductors as Cooper pairs and Bogoliubov quasiparticle excitations, whereby we modified the Bogoliubov transformation in a number conserving way<sup>25,26</sup>, introducing Cooper pair creation and annihilation operators explicitly. We showed the predictions of the theory on two examples, the well known single level quantum dot, and the double quantum dot. The characteristic gap in the Coulomb diamonds, proportional to the superconducting gap, as well as negative differential conductance was observed in both cases. Further, we considered the double quantum dot in serial as well as in parallel configuration, see Fig. 1, coupling the dots to the same as well as to two separate gate electrodes.

We systematically analyzed the stability diagrams, extending the scheme of Ref.<sup>36</sup> for superconducting leads. We found that transport through excited system states occurs even for low bias voltages using thermally excited quasiparticles, leading to zero bias peaks in the conductance. Transitions through excited states can be observed if transitions through the ground state are energetically not allowed, namely if the distance between the energy levels of the excited state and the ground state is smaller than  $2|\Delta|$ . This effect can be seen in the current voltage characteristics of an independently gated double quantum dot in parallel configuration without tuning parameters of the system, since the level spacing changes with the detuning  $\Delta_g$  of the gate voltages. Hence the excited states can be seen only in certain detuning windows. Finally, we analysed the case where a quantum dot is coupled to a normal and a superconducting lead, giving a possible explanation for the subgap features of Ref. 1 in terms of transport involving thermally excited quasiparticles.

We conclude with the observation that thermally excited quasiparticles can lead to a finite current in the Coulomb blockade region. Besides the well known thermal transitions through the ground states, transitions through excited system states must be taken into account as they are an additional source of zero bias peaks in the conductance. For a better comparison with experiments the theory can be used to investigate more realistic systems like carbon nanotube quantum double dots. Specif-

ically, the current voltage spectroscopy in the low bias regime can be used to learn something about the spectrum of the set-up. In order to observe the Josephson effect and Andreev reflections, the theory must be extended to higher order perturbation theory<sup>20,22</sup>.

## ACKNOWLEDGMENTS

We like to thank financial support through DFG Program Nos. SFB631.

## Appendix A: The BCS ground state and the Cooper pair operators

### 1. Cooper pair states

In Sect. III we claimed that a state  $|n\rangle$  contains  $2n$  electrons:

$$\hat{N}|n\rangle = 2n|n\rangle. \quad (\text{A1})$$

In order to proof this statement we need the following commutators for  $\hat{R}_q^\dagger = \hat{c}_{k\uparrow}^\dagger \hat{c}_{-k\downarrow}^\dagger$ :

$$[\hat{R}_k^\dagger, \hat{R}_q^\dagger] = 0, \quad (\text{A2})$$

$$[\hat{R}_k^\dagger, \hat{R}_q] = \delta_{kq}(\hat{c}_{k\uparrow}^\dagger \hat{c}_{k\uparrow} + \hat{c}_{-k\downarrow}^\dagger \hat{c}_{-k\downarrow} - 1), \quad (\text{A3})$$

$$[\hat{N}, \hat{R}_q^\dagger] = 2\hat{R}_q^\dagger. \quad (\text{A4})$$

In the following we proof Eq. (A1) by induction:

**Basis:**  $n = 1$

$$\hat{N}|1\rangle = \hat{N} \frac{1}{a_1} \sum_k \frac{v_k}{u_k} \hat{R}_k^\dagger |0\rangle = 2|1\rangle. \quad (\text{A5})$$

**Inductive step:**

$$\begin{aligned} \hat{N}|n+1\rangle &= \hat{N} \frac{1}{a_1} \sum_k \frac{v_k}{u_k} \hat{R}_k^\dagger |n\rangle \\ &= \frac{1}{a_1} \sum_k \frac{v_k}{u_k} \left( 2\hat{R}_k^\dagger + \hat{R}_k^\dagger \hat{N} \right) |n\rangle \\ &= 2(n+1)|n+1\rangle. \quad \square \end{aligned} \quad (\text{A6})$$

### 2. Properties of Cooper pair operators

In this paragraph we proof the properties of the Cooper pair operators which are necessary to fulfill the unitarity

of the Bogoliubov transformation. Combining Eq. (A4) with Eq. (20) we find that

$$\begin{aligned} [\hat{N}, \hat{S}^\dagger] &= 2\hat{S}^\dagger, \\ [\hat{N}, \hat{S}] &= -2\hat{S}. \end{aligned} \quad (\text{A7})$$

In Eq. (21) we have already seen that  $\hat{S}^\dagger|n\rangle = |n+1\rangle$ ; so we still have to proof the action of  $\hat{S}|n\rangle$ , using Eqs. (A7) and (A1):

$$\hat{N}\hat{S}|n\rangle = (-2\hat{S} + \hat{S}\hat{N})|n\rangle = 2(n-1)\hat{S}|n\rangle \equiv \hat{N}|n-1\rangle. \quad (\text{A8})$$

Hence we proofed that  $\hat{S}|n\rangle = |n-1\rangle$ . Acting on a test function we finally find:

$$\hat{S}\hat{S}^\dagger|\text{GS}\rangle = \sum_n b_n \hat{S}|n+1\rangle = 1|\text{GS}\rangle = \hat{S}^\dagger \hat{S}|\text{GS}\rangle, \quad (\text{A9})$$

and consequently

$$[\hat{S}^\dagger, \hat{S}]|\text{GS}\rangle = 0. \quad (\text{A10})$$

## Appendix B: Thermodynamic properties of the superconducting leads

In Sect. III A we introduced with Eq. (27) the Fermi function:

$$f^+(E) = \text{Tr}_B \left( \hat{\gamma}_{k\sigma}^\dagger \hat{\gamma}_{k\sigma} \hat{\rho}_B \right). \quad (\text{B1})$$

The situation is similar to that of a non-interacting Fermi gas, but with the BCS-ground state playing the role of the physical vacuum state. Therefore, the derivation is standard, see e.g.<sup>38</sup>. Moreover, we have to calculate thermal expectation values containing an additional Cooper pair operator:

$$\begin{aligned} \text{Tr}_B \left( \hat{\rho}_B \hat{\gamma}_{k\sigma}^\dagger \hat{\gamma}_{k\sigma} \hat{S}^\dagger \right) &= \sum_{\{n\}} \langle \{n\} | \hat{\rho}_B \hat{\gamma}_{k\sigma}^\dagger \hat{\gamma}_{k\sigma} \hat{S}^\dagger | \{n\} \rangle \\ &= \sum_{\{n\}, \{n'\}} \langle \{n\} | \hat{\rho}_B \hat{\gamma}_{k\sigma}^\dagger \hat{\gamma}_{k\sigma} | \{n'\} \rangle \langle \{n'\} | \hat{S}^\dagger | \{n\} \rangle \\ &= \sum_{\{n\}, \{n'\}} \langle \{n\} | \hat{\rho}_B \hat{\gamma}_{k\sigma}^\dagger \hat{\gamma}_{k\sigma} | \{n'\} \rangle \delta_{nn'} \langle \text{GS} | \hat{S}^\dagger | \text{GS} \rangle \\ &= \text{Tr}_B \left( \hat{\rho}_B \hat{\gamma}_{k\sigma}^\dagger \hat{\gamma}_{k\sigma} \right) \langle \text{GS} | \hat{S}^\dagger | \text{GS} \rangle. \end{aligned} \quad (\text{B2})$$

where the trace is over the many-body states defined in Eq. (28). The remaining task is to calculate the BCS-ground state expectation value of the Cooper pair operator:

$$\begin{aligned} \langle \text{GS} | \hat{S}^\dagger | \text{GS} \rangle &= \sum_{n,m} b_n b_m \langle n | \hat{S}^\dagger | m \rangle \\ &= \sum_n b_{n+1} b_n. \end{aligned} \quad (\text{B3})$$

Inserting the definition of the  $b_n$ , we obtain

$$\begin{aligned} \langle \text{GS} | \hat{S}^\dagger | \text{GS} \rangle &= \mathcal{N}^2 \sum_n \frac{(a_1)^{2n+1}}{n!(n+1)!} \\ &= \frac{I_1(2a_1)}{I_0(2a_1)}, \end{aligned} \quad (\text{B4})$$

where we used that  $\mathcal{N}^{-2} = \sum_n \frac{a_1^n}{(n!)^2} = I_0(2a_1)$ ;  $I_0$  and  $I_1$  are modified Bessel functions of the first kind<sup>39</sup>. To calculate the actual value for the expectation value, we have to evaluate  $a_1$ :

$$\begin{aligned} a_1^2 &= \sum_k \frac{|u_k|^2}{|v_k|^2} \\ &= \rho_N \int_{-\infty}^{\infty} dE \Theta(|E| - |\Delta|) \frac{|E|}{\sqrt{E^2 - |\Delta|^2}} \frac{|u_k|^2}{|v_k|^2} \\ &= 2\rho_N \int_{|\Delta|}^{\infty} dE \frac{|E|}{\sqrt{E^2 - |\Delta|^2}} \frac{|E| - \sqrt{E^2 - |\Delta|^2}}{|E| + \sqrt{E^2 - |\Delta|^2}} \\ &= 2\rho_N |\Delta| \int_1^{\infty} dx \left( \frac{2x^3}{\sqrt{x^2 - 1}} - 2x^2 - \frac{x}{\sqrt{x^2 - 1}} \right) \\ &= 2\rho_N |\Delta| \left[ \frac{2}{3} x^2 \sqrt{x^2 - 1} + \frac{1}{3} \sqrt{x^2 - 1} - \frac{2}{3} x^3 \right]_1^{\infty} \\ &= \frac{4}{3} \frac{V m k_F}{\pi^2 \hbar^2} |\Delta|. \end{aligned} \quad (\text{B5})$$

The elementary integrals can be found e.g. in Ref. 40. In the last step of Eq. (B5) we calculated the limit  $x \rightarrow \infty$  by Taylor expanding the roots. We see that  $a_1$  is proportional to  $\sqrt{V}$ , hence we find in the thermodynamic limit:

$$\langle \text{GS} | \hat{S}^\dagger | \text{GS} \rangle = \frac{I_1(2a_1)}{I_0(2a_1)} \xrightarrow{a_1 \rightarrow \infty} 1, \quad (\text{B6})$$

using the asymptotic expansion of the modified Bessel functions<sup>41</sup>:

$$I_n(x) = \frac{e^x}{\sqrt{2\pi x}} \left[ 1 + \mathcal{O}\left(\frac{1}{x}\right) \right]. \quad (\text{B7})$$

Finally we find that

$$\text{Tr}_B \left( \hat{\gamma}_{k\sigma}^\dagger \hat{\gamma}_{k\sigma} \hat{S}^\dagger \hat{\rho}_B \right) = f^+(E). \quad (\text{B8})$$

## Appendix C: Rates

### 1. Normal rates

In the stationary limit,  $\tau \rightarrow \infty$ , the normal rates read:

$$\begin{aligned} (\Gamma_{nmm'n'}^+)_\eta^{N \rightarrow N+1} &= \lim_{\tau \rightarrow \infty} \left( \frac{1}{\hbar} \right)^2 \sum_{k\sigma\alpha\alpha'} t_{\eta\alpha\sigma} t_{\eta\alpha'\sigma}^* \\ &\langle n | \hat{d}_{\alpha\sigma} | m \rangle \langle m' | \hat{d}_{\alpha'\sigma}^\dagger | n' \rangle \int_0^\tau dt_2 e^{\frac{i}{\hbar} E_{n'm'} t_2} \left[ \right. \\ &\left. |u_{\eta k}|^2 f^+(E_{\eta k}) e^{+\frac{i}{\hbar} (E_{\eta k} + \mu_\eta) t_2} + |v_{\eta k}|^2 f^-(E_{\eta k}) e^{-\frac{i}{\hbar} (E_{\eta k} - \mu_\eta) t_2} \right], \end{aligned} \quad (\text{C1})$$

$$\begin{aligned} (\Gamma_{nmm'n'}^+)_\eta^{N \rightarrow N-1} &= \lim_{\tau \rightarrow \infty} \left( \frac{1}{\hbar} \right)^2 \sum_{k\sigma\alpha\alpha'} t_{\eta\alpha\sigma} t_{\eta\alpha'\sigma}^* \\ &\langle n | \hat{d}_{\alpha\sigma}^\dagger | m \rangle \langle m' | \hat{d}_{\alpha'\sigma} | n' \rangle \int_0^\tau dt_2 e^{\frac{i}{\hbar} E_{n'm'} t_2} \left[ \right. \\ &\left. |u_{\eta k}|^2 f^-(E_{\eta k}) e^{-\frac{i}{\hbar} (E_{\eta k} + \mu_\eta) t_2} + |v_{\eta k}|^2 f^+(E_{\eta k}) e^{+\frac{i}{\hbar} (E_{\eta k} - \mu_\eta) t_2} \right]. \end{aligned} \quad (\text{C2})$$

### 2. Anomalous rates

The anomalous rates are

$$\begin{aligned} (\Sigma_{nmm'n'}^+)_\eta^{N \rightarrow N+1} &= \lim_{\tau \rightarrow \infty} \left( \frac{1}{\hbar} \right)^2 \sum_{k\sigma\alpha\alpha'} t_{\eta\alpha\bar{\sigma}}^* t_{\eta\alpha'\sigma}^* \text{sgn}(\sigma) \\ &\langle n | \hat{d}_{\alpha\bar{\sigma}}^\dagger | m \rangle \langle m' | \hat{d}_{\alpha'\sigma}^\dagger | n' \rangle v_{\eta k} u_{\eta k}^* \int_0^\tau dt_2 e^{\frac{i}{\hbar} E_{n'm'} t_2} e^{-\frac{i}{\hbar} 2\mu_\eta \tau} \\ &\left[ f^+(E_{\eta k}) e^{+\frac{i}{\hbar} (E_{\eta k} + \mu_\eta) t_2} - f^-(E_{\eta k}) e^{-\frac{i}{\hbar} (E_{\eta k} - \mu_\eta) t_2} \right], \end{aligned} \quad (\text{C3})$$

$$\begin{aligned} (\Sigma_{nmm'n'}^+)_\eta^{N \rightarrow N-1} &= \lim_{\tau \rightarrow \infty} \left( \frac{1}{\hbar} \right)^2 \sum_{k\sigma\alpha\alpha'} t_{\eta\alpha\sigma} t_{\eta\alpha'\bar{\sigma}}^* \text{sgn}(\sigma) \\ &\langle n | \hat{d}_{\alpha\sigma} | m \rangle \langle m' | \hat{d}_{\alpha'\bar{\sigma}} | n' \rangle v_{\eta k}^* u_{\eta k} \int_0^\tau dt_2 e^{\frac{i}{\hbar} E_{n'm'} t_2} e^{+\frac{i}{\hbar} 2\mu_\eta \tau} \\ &\left[ f^+(E_{\eta k}) e^{+\frac{i}{\hbar} (E_{\eta k} - \mu_\eta) t_2} - f^-(E_{\eta k}) e^{-\frac{i}{\hbar} (E_{\eta k} + \mu_\eta) t_2} \right]. \end{aligned} \quad (\text{C4})$$

From Eqs. (C3) and (C4) we can see that they contain an integral of the form:

$$\begin{aligned} \int_{-\infty}^{\infty} dE F(E) \left[ f^{(p)}(E) e^{\frac{i}{\hbar} (qE + \omega) t_2} \right. \\ \left. - f^{(-p)}(E) e^{\frac{i}{\hbar} (-qE + \omega) t_2} \right] = 0, \end{aligned} \quad (\text{C5})$$

where  $F(-E) = F(E)$  and  $p, q = \pm 1$ . The anomalous rates with the superscript ‘-’ contain the same structure, hence all anomalous rates are equal to zero.

### 3. Renormalization of the rates

In the lowest order approximation we find rates which are proportional to the BCS-density of states leading to divergences at the gap edges. We can renormalize the rates by introducing a finite lifetime  $(\gamma/\hbar)^{-1}$  in the exponents of Eqs. (C1) and Eqs. (C2). Since we are neglecting coherences the imaginary parts of the rates do not contribute to the dynamics of the system. For example consider the integral appearing in Eq. (C1):

$$\begin{aligned} & \text{Re} \left( \int_{-\infty}^{\infty} dE \int_0^{\infty} dt_2 e^{\frac{i}{\hbar}(E+\omega+i\gamma)t_2} f^+(E) D(E) \right) \\ &= \int_{-\infty}^{\infty} dE \frac{\hbar\gamma}{(E+\omega)^2 + \gamma^2} f^+(E) D(E), \end{aligned} \quad (\text{C6})$$

where we introduced  $\omega = E_{n'm'} + \mu_\eta$ . Generalizing the integral for the cases  $(N \rightarrow N \pm 1)$  it reads

$$\hbar \int_{-\infty}^{\infty} dE L(E, \omega) f^\pm(E) D(E) = \hbar \int_{-\infty}^{\infty} dE F(E), \quad (\text{C7})$$

where

$$L(E, \omega) = \frac{\gamma}{(E + \omega)^2 + \gamma^2} \quad (\text{C8})$$

describes the Lorentzian and  $F(E) = L(E, \omega) f^\pm(E) D(E)$ . We can solve the integral of Eq. (C7) using residue calculus hence. To this extend we analyze the singularities of the integrand and the area in which the integrand is analytic. The Lorentzian  $L(E, \omega)$  has poles at

$$E = -\omega \mp i\gamma, \quad (\text{C9})$$

with the corresponding residues:

$$\text{Res}_{E=-\omega \mp i\gamma} L(E) = \frac{\pm i}{2}. \quad (\text{C10})$$

The poles of the Fermi function  $f^\pm(E)$  are purely imaginary and equally distributed along the imaginary axis:

$$E = \frac{i\pi}{\beta} (2n+1) \quad n \in \mathbb{Z}, \quad (\text{C11})$$

with the residues

$$\text{Res}_{E=\frac{i\pi}{\beta}(2n+1)} f^\pm(E) = \frac{\mp 1}{\beta}. \quad (\text{C12})$$

The square roots in the BCS-density of states  $D(E)$  have branch cuts along the real axis. In Fig. 20 we sketched the contour in the complex plane which is slightly shifted away from the real axis with  $\epsilon = 1/R$ . In the limit  $R \rightarrow \infty$  the integral along the semicircle vanishes and we are left with:

$$\lim_{R \rightarrow \infty} \int_{-R}^R dx F(x + i\epsilon) = 2\pi i \sum_{\alpha} \text{Res}_{z=\alpha} F(z). \quad (\text{C13})$$

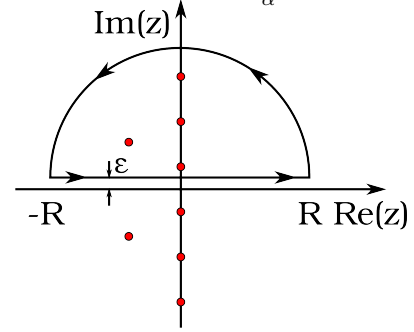


Figure 20. Contour in the complex plane used to integrate Eq. (C7).

In the limit  $R \rightarrow \infty$  Eq. (C13) is mapped back into the real integral of Eq. (C7), and we find:

$$\begin{aligned} & \hbar \int_{-\infty}^{\infty} dE L(E) f^\pm(E) D(E) \\ &= \pi \hbar \text{Re} \left( f^+(-\omega + i\gamma) D(-\omega + i\gamma) \right). \end{aligned} \quad (\text{C14})$$

\* [sebastian1.pfaller@physik.uni-r.de](mailto:sebastian1.pfaller@physik.uni-r.de)

<sup>1</sup> T. Dirks, Y.-F. Chen, N. O. Birge, and N. Mason, Appl. Phys. Lett. **95**, 192103 (2009), ISSN 00036951.

<sup>2</sup> M. Buitelaar, W. Belzig, T. Nussbaumer, B. Babić, C. Bruder, and C. Schönenberger, Phys. Rev. Lett. **91**, 057005 (2003), ISSN 0031-9007.

<sup>3</sup> E. Vecino, M. Buitelaar, A. Martín-Rodero, C. Schönenberger, and A. Levy Yeyati, Solid State Communications **131**, 625 (2004), ISSN 00381098.

<sup>4</sup> A. Eichler, M. Weiss, S. Oberholzer, C. Schönenberger, A. Levy Yeyati, J. Cuevas, and A. Martín-Rodero, Phys. Rev. Lett. **99**, 126602 (2007), ISSN 0031-9007.

<sup>5</sup> K. Grove-Rasmussen, H. I. Jørgensen, B. M. Andersen, J. Paaske, T. S. Jespersen, J. Nygård, K. Flensberg, and

P. E. Lindelof, Phys. Rev. B **79**, 134518 (2009).

<sup>6</sup> L. G. Herrmann, F. Portier, P. Roche, A. Levy Yeyati, T. Kontos, and C. Strunk, Phys. Rev. Lett. **104**, 026801 (2010).

<sup>7</sup> J.-D. Pillet, C. H. L. Quay, P. Morfin, C. Bena, a. L. Yeyati, and P. Joyez, Nature Phys. **6**, 965 (2010), ISSN 1745-2473.

<sup>8</sup> D. Ralph, C. T. Black, and M. Tinkham, Phys. Rev. Lett. **74**, 3241 (1995).

<sup>9</sup> J. A. van Dam, Y. V. Nazarov, E. P. A. Bakkers, S. De Franceschi, and L. P. Kouwenhoven, Nature **442**, 667 (2006).

<sup>10</sup> Y.-J. Doh, S. De Franceschi, E. P. A. M. Bakkers, and L. P. Kouwenhoven, Nano Lett. **8**, 4098 (2008).

<sup>11</sup> L. Hofstetter, S. Csonka, J. Nygård, and C. Schönenberger,



- Nature **461**, 960 (2009).
- <sup>12</sup> L. G. Herrmann, P. Burset, W. J. Herrera, F. Portier, P. Roche, C. Strunk, A. L. Yeyati, and T. Kontos, arXiv:1205.1972v1.
  - <sup>13</sup> C. B. Winkelmann, N. Roch, W. Wernsdorfer, and V. Bouchiat, Nature Phys. **5**, 876 (2009).
  - <sup>14</sup> G. Katsaros, P. Spathis, M. Stoffel, F. Fournel, M. Mongillo, V. Bouchiat, F. Lefloch, A. Rastelli, O. G. Schmidt, and S. De Franceschi, Nat. Nanotechnol. **5**, 458 (2010), ISSN 1748-3395.
  - <sup>15</sup> T. Dirks, T. L. Hughes, S. Lal, B. Uchoa, Y.-F. Chen, C. Chialvo, P. M. Goldbart, and N. Mason, Nature Phys. **7**, 386 (2011), ISSN 1745-2473.
  - <sup>16</sup> C. B. Whan and T. P. Orlando, Phys. Rev. B **54**, R5255 (1996).
  - <sup>17</sup> A. Levy Yeyati, J. C. Cuevas, A. Lopez-Davalos, and A. Martin-Rodero, Phys. Rev. B **55**, R6137 (1997).
  - <sup>18</sup> K. Kang, Phys. Rev. B **57**, 11891 (1998).
  - <sup>19</sup> M. G. Pala, M. Governale, and J. König, New J. Phys. **9**, 278 (2007), ISSN 1367-2630.
  - <sup>20</sup> M. Governale, M. G. Pala, and J. König, Phys. Rev. B **77**, 134513 (2008), ISSN 1550-235X.
  - <sup>21</sup> S. De Franceschi, L. Kouwenhoven, C. Schönenberger, and W. Wernsdorfer, Nat. Nanotechnol. **5**, 703 (2010), ISSN 1748-3395.
  - <sup>22</sup> A. Martín-Rodero and A. Levy Yeyati, Adv. Phys. **60**, 899 (2011).
  - <sup>23</sup> B. Andersen, K. Flensberg, V. Koerting, and J. Paaske, Phys. Rev. Lett. **107**, 256802 (2011), ISSN 0031-9007.
  - <sup>24</sup> K. J. Franke, G. Schulze, and J. I. Pascual, Science **332**, 940 (2011), ISSN 1095-9203.
  - <sup>25</sup> B. Josephson, Phys. Lett. **1**, 251 (1962), ISSN 0375-9601.
  - <sup>26</sup> J. Bardeen, Phys. Rev. Lett. **9**, 147 (1962).
  - <sup>27</sup> A. J. Leggett, F. Sols, W. G. Street, N. M. Avenue, and M. Condensada, Foundations of Physics **21**, 353 (1991).
  - <sup>28</sup> R. Pariser and R. G. Parr, J. Chem. Phys. **21** (1953).
  - <sup>29</sup> J. A. Pople, Trans. Faraday Soc. **49**, 1375 (1953).
  - <sup>30</sup> B. R. Bulka and T. Kostyrko, Phys. Rev. B **70**, 205333 (2004).
  - <sup>31</sup> R. Hornberger, S. Koller, G. Begemann, A. Donarini, and M. Grifoni, Phys. Rev. B **77**, 245313 (2008).
  - <sup>32</sup> N. N. Bogoliubov, Soviet Phys. JETP **34**, 41 (1958).
  - <sup>33</sup> M. Tinkham, *Introduction to Superconductivity: Second Edition (Dover Books on Physics)* (Dover Publications, 2004), ISBN 0486435032.
  - <sup>34</sup> K. Blum, *Density Matrix Theory and Applications: Second Edition* (Plenum Press, New York, 1996).
  - <sup>35</sup> D. S. Kosov, T. Prosen, and B. Zunkovic, arXiv:1206.3450v1.
  - <sup>36</sup> A. Donarini, G. Begemann, and M. Grifoni, Phys. Rev. B **82**, 125451 (2010), ISSN 1098-0121.
  - <sup>37</sup> W. G. van der Wiel, S. De Franceschi, J. M. Elzerman, T. Fujisawa, S. Tarucha, and L. P. Kouwenhoven, Rev. Mod. Phys. **75**, 1 (2002).
  - <sup>38</sup> A. L. Fetter and J. D. Walecka, *Quantum Theory of Many-Particle Systems* (McGraw-Hill, Inc., 1971).
  - <sup>39</sup> M. Abramowitz and I. A. Stegun, *Handbook of Mathematical Functions* (Dover Publications, Inc., New York, 1972).
  - <sup>40</sup> I. S. Gradshteyn and I. M. Ryzhik, *Table of Integrals, Series, and Products* (Academic press, 2000), 6th ed.
  - <sup>41</sup> I. N. Bronstein and K. A. Semendjajew, *Taschenbuch der Mathematik* (Harri Deutsch, 2001).